SSRG International Journal of Civil Engineering
ISSN: 2348-8352/ https://doi.org/10.14445/23488352/IJCE-V12I6P113

Volume 12 Issue 6, 151-176, June 2025

Original Article

Reliability Analysis of Unstabilized Rammed Earth Under Wind Pressure: A Hybrid Monte Carlo and Artificial Neural Network Approach

Chaymae Salhi[1], Mouna El Mkhalet[2], Nouzha Lamdouar[3]

[1,2,3]*Civil Engineering and Construction structure GCC laboratory, Mohammadia School of Engineers EMI, Mohammed V University, Rabat, Morocco.*

[1]*Corresponding Author : chaymae.salhi@research.emi.ac.ma*

Received: 10 April 2025 Revised: 15 May 2025 Accepted: 14 June 2025 Published: 28 June 2025

Abstract *- Rammed Earth (RE) is recognized as a sustainable construction material with minimal environmental impact, yet its structural reliability under lateral wind forces remains underexplored. This study evaluates the reliability of Unstabilized Rammed Earth (URE) structures using Monte Carlo Simulation (MCS) and Artificial Neural Networks (ANN)-a combination applied for the first time in RE literature. MCS was performed with 500,000 iterations to assess the structural reliability of URE and generate a dataset for ANN-based prediction of the reliability index. The analysis incorporated random variables, including compressive strength, density, roof weight and wind speed. To enhance the robustness of the MCS analysis, 95% confidence intervals for each estimated probability of failure were also computed using the Wilson score method, revealing consistently narrow bounds, which underscore the statistical stability of the simulation outcomes. The results of the MCS indicate that a wall thickness of 0.35 m satisfies the reliability requirements for the evaluated compressive strengths, whereas a thickness of 0.2 m is inadequate. The ANN model, trained on the MCS-derived dataset, achieved a strong performance with a mean squared error (MSE) of 0.023 and a coefficient of determination (R^2) of 0.853, further confirmed through 10-fold cross-validation.*

Keywords *- Unstabilized Rammed Earth, Structural Reliability, Monte Carlo Simulation, Artificial Neural Networks, Lateral wind forces.*

1. Introduction

Accounting for 36% of the world's energy consumption, the construction industry is a major contributor to environmental degradation-making adopting sustainable practices a pressing necessity across developed and developing nations [1,2]. As a result, there is a growing resurgence in building approaches that minimize environmental damage by relying on local resources such as the earth and limiting dependence on industrial production [3].

Among earth construction techniques, known historically for their efficiency, availability, and thermal and mechanical properties [3], RE stands out due to its superior mechanical strength [4], along with remarkable environmental benefits [5], making it an excellent candidate in the context of sustainable building. Historically, RE and other earth construction techniques developed through empirical optimization and understanding of the local materials [6]. In recent decades, a resurgence of interest in earth construction, including RE, has led to the development of building standards, normative documents, and guidelines [7].

Nevertheless, many critical material properties of RE remain unexplored or insufficiently investigated compared to other conventional construction techniques. They should be rigorously analyzed to achieve the same level of reliability and standardization as other construction materials like concrete and steel [3].

Earth-based construction techniques represent the earliest known building form, with Costa et al. [8] noting that examples of earth brick usage date back to approximately 10,000 BC in Mesopotamia. The RE method, in particular, is believed to have originated during the Three Kingdoms period in China (221–581 AD) and has since seen widespread application across many cultures and eras [9].

RE construction involves extracting soil compacted in successive layers within temporary molds or formwork. After each layer is firmly compressed, the formwork is repositioned-either along the wall's length or upward-allowing the structure to rise incrementally, layer upon layer [9]. RE exhibits two defining material features: it is typically compacted at or near the optimum moisture content, and its composition is poorly sorted, containing a broad range of particle sizes-from fine clay to coarse gravel-sometimes across as many as 64 distinct fractions [3, 10].

RE is generally categorized into stabilized and unstabilized forms. While Stabilized Rammed Earth (SRE) incorporates additives such as cement or lime, Unstabilized Rammed Earth (URE) relies solely on clay as a binding agent. Many studies have explored both forms, primarily through experimental methods, focusing on mechanical properties, durability, and structural performance under various loading conditions. For example, El Bourki et al. [11] experimentally evaluated the mechanical behavior of RE reinforced with varying contents of date palm fibers, using Proctor compaction, uniaxial compression, splitting tensile, and cyclic loading tests. Baibordy et al. [12] combined experimental testing with fuzzy logic modeling to assess the mechanical properties of cement- and lime-stabilized RE reinforced with straw. Xu et al. [13] examined hydrothermal migration and interface cracking in reinforced RE affected by root erosion, focusing on moisture-induced shrinkage during desiccation. Umubyeyi et al. [14] conducted a 16-year experimental assessment of the erosion and durability of URE exposed to temperate climatic conditions. Zhou et al. [15] investigated SRE's interlayer and intralayer shear properties using direct shear tests, particularly failure mechanisms and interface strength.

Other works have employed numerical modeling to assess the structural behavior of RE. For instance, Pei et al. [16] used finite element analysis to study the impact of weak interlayer interfaces on the structural performance of multi-layer discontinuous RE walls. Healy et al. [17] applied finite element modeling based on the Mohr-Coulomb failure criterion to simulate the behavior of URE, validating the model against experimental shear and compression test results. However, structural applications under lateral wind loads remain significantly underexplored. Notable exceptions include the study by Ciancio and Augarde [18], which compares elastic and ultimate strength analysis methods for evaluating lateral load capacity of unreinforced cement-stabilized RE walls, proposing a revised approach incorporating fracture energy. Additionally, Luo et al. [19] studied the deterioration of historic RE structures under wind-driven rain, aiming to correlate erosion with material properties and rain conditions through laboratory simulations.

In recent years, data-driven and probabilistic methods have complemented traditional approaches in predicting RE performance. These include machine learning, ANN, and reliability analysis techniques like the SORM (Second-Order Reliability Method) and the FORM (First-Order Reliability Method). In the context of RE, Kianfar and Toufigh [20] employed the FORM to evaluate the structural reliability of unstabilized and cement-treated RE systems under diverse loading conditions -including dead, live, and environmental loads- making it the first study that tackled the aspect of structural reliability of RE walls using reliability-based methods.

Although ANNs have been applied in RE research, these studies predominantly focus on SRE and compressive strength. For instance, Ansyz and Narloch [21] developed an ANN-based algorithm to design the composition of cement-stabilized RE in order to predict the correct moisture, cement, and soil composition needed to achieve target compressive strength levels. Another notable study by Mustafa et al. [22] investigated the unconfined compressive strength of various URE and SRE based on grain size distribution, moisture content, and stabilizer type and dosage, demonstrating ANN's superior accuracy over Multiple Linear Regression (MLR). Similarly, Ansyz et al. [23] applied ANNs, decision trees and random forests to predict the compressive strength of cement-stabilized RE, integrating explainable artificial intelligence to determine the influence of components like cement, sand, and clay. Further, Narloch et al. [24] utilized Deep Convolutional Neural Network (DCNN)-a specialized form of ANN that excels in image recognition tasks [25]-to analyze SEM (Scanning Electron Microscope) images of cement-stabilized RE, correlating microstructural features with compressive strength to reduce reliance on physical testing.

Despite these advances, no study to date has combined MCS and ANN to assess the structural reliability of RE, nor has any work explicitly focused on URE under lateral wind-induced out-of-plane loading.

To address these critical gaps, the present study offers the first integration of MCS and ANN to evaluate the structural reliability of URE walls under lateral wind loads. Compressive strength, wind speed, material density, and roof weight are modeled as random variables, while wall dimensions are treated as deterministic inputs to simulate realistic behavior. MCS is used to evaluate the structural reliability of URE walls by analyzing the interaction between compressive strength and wall thickness and to generate a synthetic dataset. This dataset is then used to train an ANN, enabling efficient prediction of the reliability index based on key parameters.

This study focuses on URE, rather than SRE, for several key reasons. By concentrating on URE, this research aims to examine the material in its pure, unaltered state, enabling a more accurate understanding of its intrinsic mechanical and physical behavior. First, as previously discussed, RE remains an under-researched construction technique, and establishing clear baseline knowledge for URE is essential for future comparative studies involving stabilized forms of RE. Second, URE holds significant traditional and local relevance, reflecting vernacular construction practices in many regions [26-29]. Studying it in its original, historical form contributes to preserving traditional knowledge and informs appropriate strategies for rehabilitating and maintaining heritage buildings constructed using this technique. Finally, there are practical and economic motivations for focusing on URE. Using stabilizers increases construction costs and depends on the availability of additives, which may be limited or require importation in remote or resource-constrained areas [6]. Therefore, URE offers a more accessible and sustainable alternative in many contexts.

Lateral loading-including wind and seismic forces-is a critical design consideration for structures in general, including RE structures [30]. It is accounted for in most existing guidelines and building standards, such as the RPCTerre [30]. However, the non-engineered nature of many earthen structures often makes them particularly vulnerable to lateral loads, especially in regions exposed to high winds [31]. Without proper reinforcement-such as continuous wall plates, bond beams, or collar beams, which enhance the lateral stability of RE walls [32]-URE constructions face a heightened risk of collapse during wind events. These vulnerabilities are especially pressing in rural, low-income, and hazard-prone areas, where URE is commonly used due to the availability and affordability of local materials [31]. In such contexts, failure of URE walls under wind loading can have severe consequences, including housing collapse, injury, displacement, and economic loss. Moreover, this structural inadequacy contributes to the perception of earthen construction as substandard, hindering its broader adoption [31]-even when it offers significant environmental and social benefits. Understanding and addressing the wind-induced failure mechanisms of URE walls is essential for improving structural resilience and enabling local communities to safely implement sustainable and affordable construction methods that meet modern safety standards and cultural needs [31].

Ultimately, this study presents a novel methodological framework that, for the first time in RE literature, combines MCS and ANN) to evaluate the structural reliability of URE walls subjected to wind-induced lateral loads. As previously discussed, while various studies have explored the mechanical behavior of stabilized and unstabilized RE under diverse loading conditions, structural applications under lateral wind loads remain significantly underexplored-particularly for URE. Building on prior work that employed probabilistic methods like FORM and data-driven models like ANNs, this research uniquely integrates the two approaches to address a critical gap. By modeling key parameters-such as compressive strength, wind speed, material density, and roof weight-as random variables and using MCS-generated data to train an ANN, the study provides a reliable and computationally efficient tool for predicting failure risk. Compared to FORM-based approaches, the MCS-ANN model demonstrates superior flexibility in handling nonlinear interactions between variables. In doing so, it advances the methodological landscape of RE analysis. It contributes to the broader goals of sustainable construction by supporting the safe implementation of affordable, low-carbon building systems in wind-exposed and resource-constrained settings.

2. Methods

This research adopts a two-phase methodology to assess the structural reliability of URE under lateral wind loads. The first phase involves an MCS for probabilistic analysis, while the second phase applies ANN to predict the reliability index based on the simulation outcomes.

The first part consists of conducting MCS on 500,000 iterations using Python in the PyCharm environment based on input data compiled from technical documents and literature. The primary objective of the MCS was twofold: first, to generate a robust dataset for training the ANN, and second, to explore the interaction between compressive strength and wall thickness in the context of structural reliability. This interaction analysis allows for deriving practical design recommendations regarding the minimum compressive strength required for each wall thickness assessed. The simulation is based on data compiled from existing technical documents and standards. The limit state function is established based on the principles of elastic analysis as outlined in the work of Ciancio and Augarde [18] and the French Snow and Wind Load Regulations (NV65) [33]. The results from the simulation were exported to Microsoft Excel for readability and further processing. Additionally, 95% confidence intervals for the estimated probabilities of failure were computed using the Wilson score method to assess the statistical reliability of the simulation results.

The simulation includes both random and deterministic input parameters. In contrast to deterministic analysis-which typically relies on fixed worst-case values-reliability analysis incorporates variability and uncertainty in both material properties and applied loads [20]. In this context, random variables were selected to reflect real-world variability. The selected random variables-compressive strength, wind speed, roof weight, and material density-were chosen based on their known practice variability and significant influence on structural reliability, as commonly reported in the literature [20]. The deterministic variables-the wall dimensions-were fixed to maintain a focused study scope. However, investigating the effect of their uncertainty would be a valuable direction for future research.

The roof weight is modeled with a normal distribution, having a mean of 1.5×10^{-3} MN/m² and a Coefficient Of Variation (COV) of 7%. The compressive strength is modeled as a lognormal distribution with a COV of 35% and evaluated at several values: 0.4, 0.5, 0.6, 1.0, 1.5, 2.0, and 2.5 MPa. A Gumbel distribution represents wind speed, considering a peak value of 36.11 m/s and a COV of 50%. The density is assumed to follow a normal distribution, with a mean value of 1900 kg/m³ and a COV of 7%. Wall thickness was treated as a deterministic parameter in the analysis (assessed at 0.2, 0.225, 0.25, 0.3, 0.4, 0.45, and 0.5 meters), wall height (3 meters), wall length (4 meters), and the span between load-bearing walls (6 meters).

The second phase of the methodology involves developing a predictive model using ANN. A dataset derived from the MCS results is selected, normalized, and used to train the network. The ANN is implemented using MATLAB's Neural Network Toolbox, applying a feedforward architecture with a Levenberg-Marquardt backpropagation algorithm. An 80-10-10 split is applied to the dataset for training, validation, and testing. The model utilized the Rectified Linear Unit (ReLU) as its activation function, with a learning rate of 0.001 and a regularization parameter of 0.01. To prevent overfitting, early stopping is applied with patience of 6 epochs.

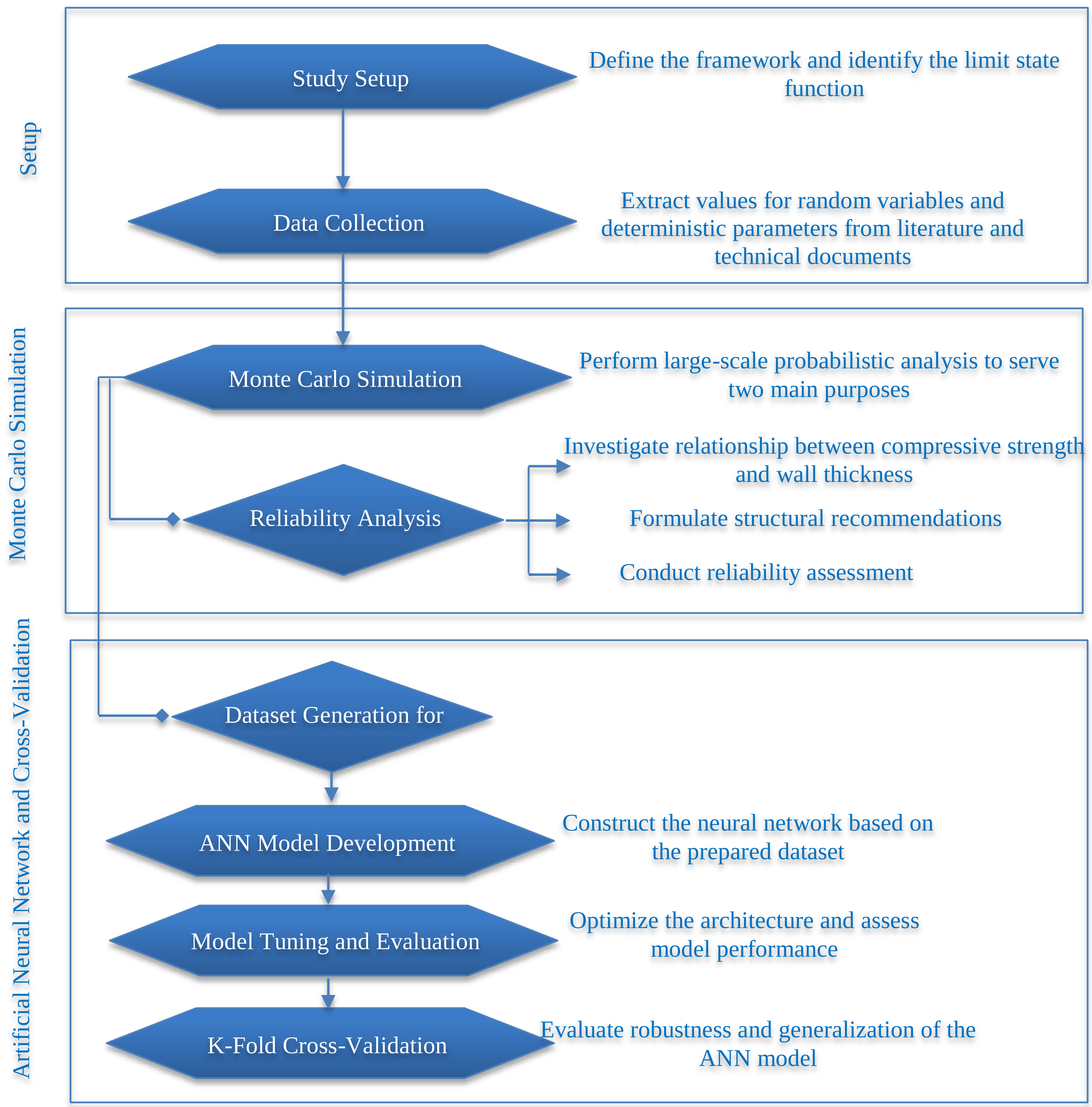

Fig. 1 Methodology flowchart illustrating the three-phase process: initial setup, monte carlo simulation, and artificial neural network-based prediction with cross-validation

Several network configurations are evaluated. Architectures with two and three hidden layers were tested, with the number of neurons per layer ranging from 1 to 12 for the two-layer models and 1 to 15 for the three-layer models. Model performance is assessed based on Mean Squared Error (MSE) and the coefficient of determination (R^2). After identifying the best-performing configuration, k-fold cross-validation is conducted to ensure the robustness and generalization capability of the trained network. This two-phase methodology allows the probabilistic assessment of structural performance and the efficient prediction of reliability based on input parameters. Figure 1 provides a visual overview of the methodological process through a detailed flowchart.

3. Results

3.1. Literature Review

3.1.1. Structural Reliability Analysis

Structural Reliability Analysis (SRA) involves a structured approach to evaluating uncertainties and probabilistic variables that influence structural design, maintenance strategies, inspections, and engineering decisions [34]. The main purpose of SRA is to evaluate and ensure structural safety by incorporating all sources of variations in load and resistance parameters and assessing their influence on the structure's performance.

[35, 36]. This places SRA as a prominent component of Structural design and optimization [37], particularly in civil engineering, a discipline characterized by expert judgement, partial knowledge, and uncertain factors inherent in the manufacturing process and the life cycle of structures [38, 39]. This is particularly relevant to RE structures, making SRA a crucial aspect to incorporate into their analysis, especially given the limited research in this area. The steps of the SRA process are illustrated in Figure 2 based on the procedure presented in the study by Song and Zhang [37].

Practically, SRA aims to determine the failure probability [39]. However, except for certain cases, the integral for failure probability (defined in Equation 1) is usually analytically intractable, owing to the complexity embedded within the limit state function [40]. Consequently, developing efficient numerical methods for generating approximate solutions remains a key focus for researchers, as demonstrated in various studies, including those by Bucher and Bourgund [41], H. Xu and Rahman [42], and J. Xu and Zhu [43].

$$P_f = \int_x I(g(x)f_X(x)dx \qquad (1)$$

Where

- $X = [X_1, X_2, \ldots, X_d]^T \in \chi \subset \mathbb{R}^d$ represent a group of fundamental random variables governed by a known joint probability density function (PDF) $f_X(x)$;
- $x = [x_1, x_2, \ldots, x_d]^T$ denotes a specific realization of X;
- $g(.)$ is the limit state function, commonly known as the performance function, defining the boundary between states of safety and failure and taking a value less than zero to indicate failure;
- $I(.)$ represents the failure indicator function, defined as $I(g(x)) = 1$ if $g(x) < 0$ (indicating failure) and $I(g(x)) = 0$ otherwise.

Numerical methods existing in literature are generally classified into five categories [44]: stochastic simulations, asymptotic approximations, moment-based approaches, probability-conservation methods and surrogate model-assisted strategies. Stochastic simulation methods, for instance, include techniques such as MCS and its variants, while asymptotic approximation methods encompass approaches like the FORM and the SORM [45].

On the other hand, methods of moments include, among others, second-moment methods, which encompass techniques such as the First-Order Second-Moment method (FOSM) and the Hasofer-Lind method [46]. Furthermore, probability-conservation methods feature techniques with two common examples: the probability density evolution method and the direct probability integral method [40]. Lastly, surrogate-assisted methods, which in the context of reliability analysis represent metamodels, include a variety of techniques and their variants, like Kriging, ANN and Support Vector Machines (SVM) [47].

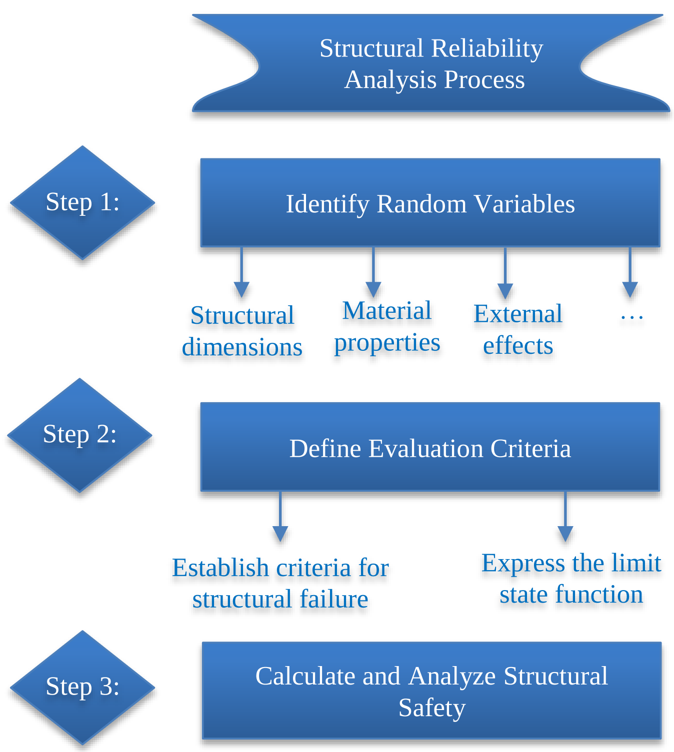

Fig. 2 Flowchart of structural reliability analysis steps adapted from the study by Song and Zhang [37]

3.1.2. Monte Carlo Simulation

In the present work, we direct our attention solely to the MCS. Initially proposed in 1949 by Metropolis and Ulam [48], the MCS, regardless of being recognized as a method with high computational cost [49], is regarded as the earliest, most broadly adopted, and trusted simulation technique for assessing the failure probability, employing random sampling drawn from each variable's PDF [50].

MCS is widely used in various disciplines, including environmental science [51-53], physics and astronomy [54, 55], medicine and dentistry [56, 57] and engineering [58-60]. In the realm of civil engineering, MCS is employed in several contexts. For instance, Smakosz et al. [61] used a Monte Carlo simulation-based material model to analyze the fracture resistance of asphalt pavement layer, focusing on the probabilistic nature of cracking in pavement overlays. Similarly, Chen et al. [62] developed an efficient algorithm using MCS to assess the elastic buckling of corroded I-section steel members, addressing computational challenges in traditional finite element analysis. Additionally, Löfman and Korkiala-Tanttu [63] investigated how clay compressibility and over-consolidation uncertainty impact settlement predictions for transportation infrastructure, using both FOSM and MCS, ultimately concluding that MCS offers greater precision.

3.1.3. Artificial Neural Networks

ANNs are algorithmic frameworks that mimic the mechanisms of biological systems [64]. The foundational work in this field occurred in the late 19th and early 20th centuries [64]. Significantly, McCulloch and Pitts (1943) introduced the first mathematical mode of neurons to elucidate nerve activity, while Rosenblatt [66] presented the first actual ANN [22].

ANNs are widely applied to advance applications in both business and scientific domains [67]. In scientific domains, ANNs have found applications across various sectors, from aerospace and electronics to telecommunications, transportation, and the environment [64]. ANN-based models are widely used in engineering disciplines, particularly civil and structural engineering [68]. There have been contributions in different aspects, according to the study by Lagaros [68], such as earthquake engineering and design codes [69-71], structural optimization and decision making [72-74], material properties and performance [75-77] as well as geotechnical engineering [78-80].

3.2. Case Study

3.2.1. Development of the Limit State Function

Mathematical Development of the Limit State Function

Ciancio and Augarde [18] examined two analytical approaches for estimating the load-bearing capacity of RE walls subjected to lateral wind forces, with particular emphasis on unreinforced cement-stabilized RE. The initial method relies on elastic analysis, whereas the second utilizes ultimate strength principles. The results suggest that elastic analysis can effectively estimate both the maximum wind pressure a rammed earth wall can endure and the point at which cracking is likely to begin during failure. In contrast, the ultimate strength analysis considerably underestimates the wall's capacity to resist wind load prior to failure.

Consequently, given the context of this study, the maximum wind pressure that the wall can resist, as proposed in their elastic analysis, is adopted to develop the limit state function. The former is expressed such as [18]:

$$w_{f_{max}} \frac{5Pt+2dt^2(f_t+2h\gamma)+2t\sqrt{(P+dtf_t)(4P+dt(f_t+4h\gamma))}}{3dh^2} \tag{2}$$

Where *h*, *t* and *d* are the height, thickness and length of the wall, P is the weight of the roof, f_t is the tensile strength, and γ is the unit weight of the material.

Consequently, the limit state function can be defined as follows:

$$g(X) = w_f - w_{f_{max}} \tag{3}$$

Where w_f denotes the applied wind pressure, and X represents the vector of random variables. The performance function $g(X)$ characterizes the system state, where $g(X) < 0$ indicates a safe state, $g(X) = 0$ defines the limit state (on the set of failures), and $g(X) > 0$ corresponds to failure.

Analytical Transformation of the Limit State Function

Tensile Strength f_t: Despite the tensile strength being one of the most pertinent mechanical parameters in the analysis of rammed earth, it is often disregarded and overlooked in the existing literature [3]. Studies exploring the tensile strength concluded that it can be considered approximately 10% of its compressive strength [3]. This is according to the guidelines of the RPCTerre [30], which proposes that the tensile strength in the absence of experimental data is 0.1 of the compressive strength. Consequently, we express in this study the tensile strength as:

$$f_t = 0.1 f_c \tag{4}$$

Unit Weight of Rammed Earth γ : The unit weight of materials is expressed in Equation 5 such as:

$$\gamma = \rho \times g \tag{5}$$

Where ρ is the density of the material and g is the acceleration due to gravity (9.81 m/s²).

Applied Wind Pressure w_f: According to the French Snow and Wind Load Regulations (NV65) [33], the wind pressure on one of the faces of the wall is given by the expression in Equation 6:

$$w_f = cq \tag{6}$$

Where q corresponds to the dynamic pressure, c represents the pressure coefficient.

Building geometry, façade detailing, wind speed and direction, among other parameters, affect the wind pressure [81]. According to Ciancio and Augarde [18], the wind is assumed to be uniformly distributed along the height of the wall, overlooking both the internal negative pressure and the uplifting force generated by the wind. A schematic inspired by their study, illustrating the loading, limit conditions, and the expected elastic deformation pattern considered in their analysis, is presented in Figure 3.

Since this study is focused on assessing the performance of URE under lateral wind pressure in a generalized framework rather than a detailed examination of a specific structure, the parameters influencing the pressure coefficient are not critical for our purposes. Consequently, this paper does not consider the pressure coefficient to simplify the limit state function. Therefore, the dynamic pressure is taken to be equal to the wind pressure, as defined as suggested by the NV65 [33] in Equation 7:

$$w_f = q = \frac{w_s{}^2}{16.3} daN/m^2 \tag{7}$$

Where w_s represents the wind speed.

Complete Expression of the Limit State Function

Taking the above into account, and after verifying unit consistency, the limit state function is defined as follows (to enhance clarity and presentation, the limit state function is split across two lines, given the complexity of the expression):

$$\begin{aligned} g(X) = {} & \frac{w_s{}^2 \times 10^{-5}}{16.3} - \frac{15\,dPt + 2\,dt^2(f_c + 2\times10^{-6}\,hrg)}{3\,dh^2} \\ & - \frac{2t\sqrt{(3dP + 0.1f_c dt)(12\,dP + dt(0.1f_c + 4\times10^{-6}\,hrg))}}{3\,dh^2} \end{aligned} \tag{8}$$

3.2.2. Characterization of Random Variables

Compressive strength f_c

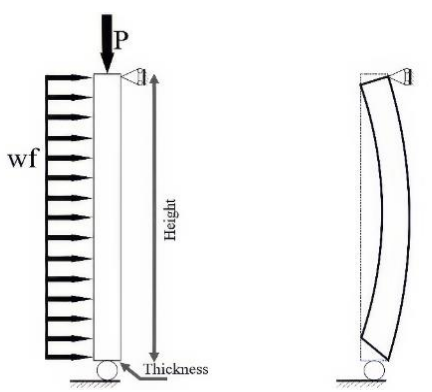

Fig. 3 Illustration of the Elastic Analysis Setup, Indicating the Boundary Conditions (Left) and the Expected Elastic Deformation Pattern (Center), Based on the Study by Ciancio and Augarde [18]

Compressive strength is defined as the maximum compression load specimens can withstand before their rupture, divided by the specimens' cross-sectional area [82]. This mechanical property is fundamental for structural materials [83]. It represents the most essential and required mechanical characteristic for several materials, such as ceramic materials [84], concrete and mortar [85], as well as for brittle materials, including RE [3].

Based on the reviewed standards, normative documents, and building codes, the specified values for compressive strength of URE range from 0.4 to 2.07 MPa, as summarized in Table 1. For instance, the RPCTerre [30] recommends a minimum characteristic compressive strength of 0.5 MPa, also adopted by the New Zealand standard NZS 4297:1998 [86]. The Zimbabwean Code of Practice for RE Structures (TH03) [87] sets a minimum average compressive strength of 1.5 MPa for general cases, increasing to 2 MPa for walls with heights between 3 and 6 meters. Similarly, Kianfar and Toufigh [20] specify a minimum compressive strength of 2 MPa for URE with a COV of 35%. The Australian normative documents, Bulletin 5 [88], and HB 195-2002 [89] recommend a design value for characteristic compressive strength of 0.7 MPa and 0.4-0.6 MPa, respectively. The American building code 14.7.4 NMAC [90] sets a minimum of approximately 2.07 MPa (300 psi) for the ultimate compressive strength of RE structures.

To model the compressive strength of URE, the lognormal distribution has been identified as the most appropriate probabilistic representation [91]. Accordingly, this study will assess a range of mean compressive strengths-0.4 MPa, 0.5 MPa, 0.6 MPa, 1 MPa, 1.5 MPa, 2 MPa and 2.5 MPa-using a lognormal distribution to reflect the variability observed in practice, characterized by a COV of 35%.

Wind Speed w_s

In the study by Kianfar and Toufigh [20], wind speed is treated as a random variable with a maximum value of 130 km/h and a COV of 50%. A Gumbel distribution was adopted to model its variability. Costa and Beck [92] explain that in EN 1990:2002 (Eurocode- Basis of Structural Design) [93], characteristic values for climatic actions, including wind and snow, are defined based on a 2% annual probability of exceedance, which corresponds to a mean return period of 50 years.

In the Moroccan context, studies providing data on maximum wind speed are limited. One notable study by Nfaoui et al. [94] reported average wind speeds across various regions, highlighting that the Taza region and parts of the far south and north of Morocco experience the highest wind speeds. Among the regions studied, the highest wind speed was recorded in Dakhla, with a speed of 11.2 m/s (40.32 km/h). Another series of studies examined wind speed patterns in Morocco by providing model projections. The first, conducted by Khokhlov and El Hadri [95], covers 2020 and

2050 and estimates a future maximum daily wind speed of 11.8 m/s (42.48 km/h) near Dakhla on the Atlantic coast. The second study [96], focused on the Tangier region between 2021 and 2050, projects a peak wind speed of 11 m/s (39.6 km/h) at the Koudia El Baida station near Tetouan.

Beyond academic studies, limited sources provide data on maximum wind speeds in Morocco. However, according to press reports, the General Directorate of Meteorology recorded an extreme wind speed of 115 km/h in Oujda on March 24th, 202.

In aligning with the Moroccan context, this study adopts a maximum value of 115 km/h (31.94 m/s), assuming a 2% probability of exceedance and a mean return period of 50 years. The Gumbel distribution is employed to model this extreme value, assuming a COV of 50%.

The Weight of the Roof P

For the roof dead loads, Kianfar and Toufigh [20] recommend a mean value of 1.5 kN/m², a COV of 7% and a normal distribution based on the guidelines of the Chinese uniform standard for building structures GJB 68-84. Although studies such as Baglioni et al. [97] have explored building materials and multilayered RE roof systems, specific data regarding the density and thickness of roof layers-as well as the density of earth used in RE walls- remain scarce within the Moroccan context. This lack of localized data complicates the region's accurate estimation of roof weight. Consequently, this study adopts the values recommended by Kianfar and Toufigh [20].

Table 1. Compressive Strength Recommendations for Rammed Earth as Provided in Various Technical Documents

Country	Ref.	Id	Type	Compressive strength (MPa)
Morocco	[30]	RPCTerre	Building code	0.5
Zimbabwe	[87]	Rammed Earth Structures (code for practice TH03)	Standard	1.5-2
Australia	[88]	Bulletin 5	Normative document	0.7
Australia	[89]	HB 195-2002	Normative document	0.4-0.6
New Zealand	[86]	NZS 4297:1998	Standard	0.5
USA	[90]	14.7.4 NMAC	Building code	2.07
Iran	[20]	-	Paper	2

Density ρ

The literature reports a wide range of density values for URE, typically between 1750 kg/m³ to 2200 kg/m³ [3]. Based on the synthesis of available research, Kianfar and Toufigh [20] have a mean of 1900 kg/m³ and a COV of 7% and-values consistent with those reported in the existing literature. Accordingly, this study adopts the values recommended by [20] for modeling purposes.

Table 2 summarises the random variables used in the analysis, including their probability distributions and corresponding statistical parameters.

3.2.3. Specification of Other Parameters

Thickness t

In the case of RE structures, wall thickness is a fundamental factor investigated in existing technical documents, including standards and academic papers. The minimum wall thickness plays a critical role in determining the performance of RE walls [20].

The study by Baglioni et al. [97] conducted a study on traditional buildings utilizing RE in Morocco, focusing on the RE buildings in the Drâa Valley. They reported that rammed earth buildings typically have a 45-50 cm thickness. In France, as reported by Bui et al. [98], a typical thickness of 50 cm is standard for both traditional and contemporary RE constructions. Reyes et al. [29], Their study, which was conducted on typical earthen houses in Colombia, including RE, reported variations in wall thickness, ranging from 40 to 100 cm, with a typical value of 60 cm. In the Moroccan context, the RPCTerre [30] recommend a minimum thickness of 40 cm for bearing rammed earth walls.

According to the several technical documents we reviewed, the minimum wall thickness recommended varies between 0.2 m and 0.457 m. The Australian standard HB 195-2002 [89] and the study by Kianfar and Toufigh [20] provide a minimal wall thickness recommendation for external and internal RE walls. However, in this study, we will focus specifically on external load-bearing RE walls. The values specified in the technical document reviewed are presented in Table 3.

Based on these considerations, this study evaluates the following wall thicknesses: t=0.2 m, 0.225 m, 0.25 m, 0.3 m, 0.35m, 0.4 m, 0.45 m and 0.5 m.

Geometric Parameters: Height h, Length d, and Wall Span

Technical documents often link recommendations for maximum wall height to wall thickness. For instance, Thompson et al. [7] suggest a wall height of 2.4m, based on a commonly applied ratio of wall height to thickness 8:1, assuming a thickness is 0.3m. Similarly, the American building code 14.7.4 NMAC [90] bases its height recommendations on wall thickness and spectral response acceleration at short periods, resulting in allowable heights ranging from 3 m to 3.6 m. Other technical documents offer specific limits. According to NZS 4297 [86], the total height of an earthen wall, including the gable end, should not exceed 6.5 m. The NBC 204:2015 [99] specifies that the floor-to-floor height for earthen buildings should range from 1.8 m to 2.5 m. In the Moroccan context, the RPCTerre [30] recommends a maximum height of 4 m for single-storey earthen structures. Baglioni et al. [97] note that traditional RE buildings in Morocco have floor heights varying from 2.5 m to 5 m. In France, El-Nabouch et al. [100] report that story heights average around 3 m, a value also used by Bui et al. [101] in their study.

In contrast, recommendations for the length of walls are less common in technical documents. Among the ones reviewed, only a few explicitly address this dimension. HB 195-2002 [89] and NBC 204:2015 [99] recommend maximum wall lengths of fifteen and ten times the wall thickness for unsupported walls, respectively. For supported walls, Arya [102] and IS 13837 [103] suggest a limit of 10 times the thickness, while NZS 4297 [86] allows up to 12 meters. The Nigerian building code NBC 10.23 [104] specifies a maximum unsupported wall length of 3.65 m. In France, El-Nabouch et al. [100] RE walls typically range between 3 to 4.5 m in length, and Bui et al. [101] modeled walls with a length of 3 m in their analysis.

Table 2. Selected random variables with their probability distributions and statistical parameters used in the monte carlo simulation

Random Variable		Distribution	Mean value	Maximum value	Coefficient of variation (%)	Standard deviation
$\boldsymbol{P}$ (MN/m²)	**Roof Weight**	Normal	1.5×10^{-3}	-	7	1.05×10^{-4}
$\boldsymbol{f_c}$ (MPa)	**Compressive strength**	Lognormal	0.4 0.5 0.6 1 1.5 2 2.5	-	35	-
$\boldsymbol{w_s}$ (m/s)	**Wind speed**	Gumbel	-	36.11	50	-
$\boldsymbol{\rho}$ (kg/m³)	**Density**	Normal	1900	-	7	133

Table 3. Summary of wall thickness recommendations in reviewed technical documents for rammed earth construction

Country	Ref.	Id	Type	t (m)
Morocco	[30]	RPCTerre	Building code	0.4
Afghanistan	[102]	GERDCRBA	Normative document	0.3
Australia	[89]	HB 195-2002	Normative document	0.2
India	[103]	IS 13837:1993	Standard	0.3
Nepal	[99]	NBC 204:2015	Building code	0.4-0.45
New Zealand	[86]	NZS 4297	Standard	0.25-0.35
USA	[90]	14.7.4 NMAC	Building code	0.457
Nigeria	[104]	NBC 10.23	Building code	0.225
Zimbabwe	[87]	Rammed Earth Structures (code for practice TH03)	Standard	0.3
Iran	[20]	-	Paper	0.25-0.3
Ireland/UK	[7]	-	Paper	0.3

Specifications concerning the span between load-bearing walls are also limited across existing technical documents. NBC 10.23 [104] states that unsupported spans-i.e., without columns, beams, or intermediate supports-should not exceed 7m. The RPCTerre [30] specifies that the span between two load-bearing walls must not exceed either ten times the wall's thickness or the value given by $64t^2/h$. Several studies on RE structures have adopted a typical load-bearing span of 6 m [100, 105]. Table 4 summarizes the recommendations from existing technical documents for wall height, length, and span between load-bearing walls, providing a clear overview of these specifications. Since this study focuses on evaluating the reliability and structural integrity of RE buildings under lateral wind pressure within a generalized context, recommendations conditional on other geometric parameters (such as height, span, or thickness) are not directly applicable. Therefore, a representative configuration is adopted to ensure the study remains applicable to various design scenarios while remaining consistent with standard practice in conventional residential construction and maintaining good living conditions.

Accordingly, a wall height of 3 m, a length of 4 m, and a span of 6 m between load-bearing walls are used for the analysis. Table 5 regroups the final values assessed in the study for wall height, length, and span between load-bearing walls. The study also considers random variables, with specifications based on existing technical documents. These recommended ranges from the literature are used to conduct simulations, which are then reevaluated through a reliability-based approach. This ensures that the dataset generated reflects actual, literature-supported ranges and can be used to train an ANN for further analysis.

3.2.4. Target Reliability Index

The probability of failure (P_f) is linked to the reliability index (β) via the Cumulative Distribution Function (CDF) of the standard normal distribution, such that $P_f = \Phi(-\beta)$, where Φ denotes the standard normal CDF [106]. In SRA, the primary objective is to verify that the probability of failure does not exceed an acceptable limit or that the reliability index exceeds a specified target value [20].

There are no specific recommendations in the literature regarding target reliability indices for RE. As a result, this study adopts a target reliability index of 3.8, following guidance provided for unreinforced masonry structures [107]. Additionally, in scenarios where the computed probability of failure is zero, a nominal value of 10^{-6}-corresponding to a reliability index of approximately 5.61-is assigned to enable consistent graphical representation and interpretation of results.

3.3. Application

3.3.1. Monte Carlo Simulation

Code Validation Process

To validate the MCS code-developed in Python and executed in the PyCharm environment with 500,000 iterations for each combination of thickness (t) and compressive strength (f_c)-Python's unit test module implements a structured three-phase validation process. The choice of 500,000 iterations ensures high accuracy in the estimated results, as the literature suggests that simulation runs within the range of 100,000 to 500,000 are generally sufficient to produce reliable estimates [108]. The validation consisted of the following steps:

Phase 1: Validation of Random Variable Generators: At this stage, the generated values were checked to ensure they accurately reflected the intended statistical properties, aligning with the characteristics of Gumbel, normal, and lognormal distributions.

Phase 2: Integration Testing: The complete script was tested by executing simulations across all combinations of wall thickness (t) and compressive strength (f_c) using 1,000 iterations to reduce computational time. The output was verified to confirm that the computed failure probabilities consistently fell within the valid range [0, 1].

Phase 3: Accuracy Testing: This phase involved validating the precision of the limit state function outputs by comparing computed results against expected analytical values derived directly from the limit state function.

All three phases were completed, confirming the correctness and reliability of the code implementation.

Results of the Simulation

The raw results of the MCS are presented in Table 6 and Table 7, which report the computed values of the reliability index and the probability of failure, respectively, for one-storey URE walls across varying wall thicknesses and compressive strengths. The reliability index results are also graphically represented in Figure 4 to enhance interpretation.

Confidence Intervals

In statistics, a confidence interval defines a range within which the actual value of an estimated parameter is likely to fall with a specified level of confidence [109]. In this study, the probability of failure is treated as a binomial proportion, resulting from a fixed number of independent Bernoulli trials-each representing either failure or survival of the structure [110].

The confidence intervals for the estimated failure probabilities were computed using the Wilson score interval method, which improves accuracy over the traditional Wald method-especially for rare events or small failure probabilities [110]. The formula used is as follows in Equation 9:

$$CI = \frac{(2nP_f + z^2) \pm z\sqrt{z^2 + 4nP_f(1-P_f)}}{2(n+z^2)} \quad (9)$$

Where n is the number of samples (in this case, 500,000), P_f is the estimated probability of failure, and z denotes the z-score associated with the selected confidence level. This study adopts a 95% confidence level, as it is commonly used in engineering applications [109]. This level implies a 5% chance that the actual probability of failure lies outside the computed interval [109]. Table 7 includes the 95% confidence intervals related to the probability of failure for each case.

Table 4. Geometric specifications-wall height, wall length, and span between load-bearing walls-from existing rammed earth technical documents

	ID	Reference	Specified values
Wall Height	-	[7]	2.4
	14.7.4 NMAC	[90]	3 – 3.6
	NZS 4297	[86]	6.5[a)]
	NBC 204:2015	[99]	2.5
	RPCTerre	[30]	4[a)]
	-	[97]	2.5 - 5
	-	[100]	3
	-	[101]	3
Wall Length	HB 195-2002	[89]	≤15 t
	NBC 204:2015	[99]	≤10 t
	Arya	[102]	≤10 t
	IS 13837	[103]	≤10 t
	NZS 4297	[86]	12
	NBC 10.23	[104]	3.65
	-	[100]	3 – 4.5
	-	[101]	3
Span between load-bearing walls	NBC 10.23	[104]	7
	RPCTerre	[30]	$\begin{cases} \leq 10\,t \\ \leq 64t^2/h \end{cases}$
	-	[100]	6

a) Represent maximum recommended limits, while the remaining values are standard recommendations provided in the respective technical documents

Table 5. Representative wall dimensions-height, length, span, and thickness-used in the reliability analysis

Parameters	Thickness t (m)	Height h (m)	Length d (m)	Wall Span (m)
Assessed Values	0.2	3	4	6
	0.225			
	0.25			
	0.3			
	0.35			
	0.4			
	0.45			
	0.5			

Table 6. Monte carlo simulation results: reliability index values for each combination of wall thickness and compressive strength

		Thickness t (m)							
		0.2	**0.225**	**0.25**	**0.3**	**0.35**	**0.4**	**0.45**	**0.5**
Compressive strength f_c (MPa)	**0.4**	2.679	2.933	3.171	3.622	3.933	4.465	5.612	5.612
	0.5	2.74	2.995	3.253	3.746	4.065	4.611	5.612	5.612
	0.6	2.818	3.069	3.337	3.781	4.132	5.612	5.612	5.612
	1	3.058	3.363	3.54	4.046	4.465	5.612	5.612	5.612
	1.5	3.287	3.568	3.757	4.224	5.612	5.612	5.612	5.612
	2	3.435	3.769	4.013	5.612	5.612	5.612	5.612	5.612
	2.5	3.626	3.921	4.107	5.612	5.612	5.612	5.612	5.612

Table 7. Probability of failure and 95% confidence intervals from monte carlo simulation for the wall thickness and compressive strength combinations assessed

Compressive strength f_c (MPa)		Thickness t (m): 0.2	0.225	0.25	0.3	0.35	0.4	0.45	0.5
0.4	P_f	0.3694	0.168	0.076	0.0146	0.0042	0.0004	10^{-6}	10^{-6}
0.4	CI*	[0.3681, 0.3707]	[0.1670, 0.169]	[0.0753, 0.0767]	[0.0143, 0.0149]	[0.004, 0.0044]	[0.0003483, 0.0004594]	[1.044×10^{-7}, 9.579×10^{-6}]	[1.044×10^{-7}, 9.579×10^{-6}]
0.5	P_f	0.3072	0.1372	0.057	0.009	0.0024	0.0002	10^{-6}	10^{-6}
0.5	CI	[0.3059, 0.3085]	[0.1362, 0.1382]	[0.0564, 0.0576]	[0.0087, 0.0093]	[0.0023, 0.0025]	[0.0001645, 0.0002432]	[1.044×10^{-7}, 9.579×10^{-6}]	[1.044×10^{-7}, 9.579×10^{-6}]
0.6	P_f	0.2416	0.1074	0.0424	0.0078	0.0018	10^{-6}	10^{-6}	10^{-6}
0.6	CI	[0.2404, 0.2428]	[0.1065, 0.1083]	[0.0418, 0.043]	[0.0076, 0.008]	[0.0017, 0.0019	[1.044×10^{-7}, 9.579×10^{-6}]	[1.044×10^{-7}, 9.579×10^{-6}]	[1.044×10^{-7}, 9.579×10^{-6}]
1	P_f	0.1114	0.0386	0.02	0.0026	0.0004	10^{-6}	10^{-6}	10^{-6}
1	CI	[0.1105, 0.1123]	[0.0381, 0.0391]	[0.0196, 0.0204]	[0.0025, 0.0027]	[0.0003483, 0.0004594]	[1.044×10^{-7}, 9.579×10^{-6}]	[1.044×10^{-7}, 9.579×10^{-6}]	[1.044×10^{-7}, 9.579×10^{-6}]
1.5	P_f	0.0506	0.018	0.0086	0.0012	10^{-6}	10^{-6}	10^{-6}	10^{-6}
1.5	CI	[0.05, 0.0512]	[0.0176, 0.0184]	[0.0083, 0.0089]	[0.0011, 0.0013]	[1.044×10^{-7}, 9.579×10^{-6}]	[1.044×10^{-7}, 9.579×10^{-6}]	[1.044×10^{-7}, 9.579×10^{-6}]	[1.044×10^{-7}, 9.579×10^{-6}]
2	P_f	0.0296	0.0082	0.003	10^{-6}	10^{-6}	10^{-6}	10^{-6}	10^{-6}
2	CI	[0.0291, 0.0301]	[0.008, 0.0085]	[0.0029, 0.0032]	[1.044×10^{-7}, 9.579×10^{-6}]	[1.044×10^{-7}, 9.579×10^{-6}]	[1.044×10^{-7}, 9.579×10^{-6}]	[1.044×10^{-7}, 9.579×10^{-6}]	[1.044×10^{-7}, 9.579×10^{-6}]
2.5	P_f	0.0144	0.0044	0.002	10^{-6}	10^{-6}	10^{-6}	10^{-6}	10^{-6}
2.5	CI	[0.0141, 0.0147]	[0.0042, 0.0046]	[0.0019, 0.0021]	[1.044×10^{-7}, 9.579×10^{-6}]	[1.044×10^{-7}, 9.579×10^{-6}]	[1.044×10^{-7}, 9.579×10^{-6}]	[1.044×10^{-7}, 9.579×10^{-6}]	[1.044×10^{-7}, 9.579×10^{-6}]

*Note: CI=Confidence Interval

3.3.2. Artificial Neural Networks

Rationale for Dataset Selection

In this paper, instead of just considering random variables and conducting MCS, a range of values for both thickness (t) and compressive strength (f_c) was considered, and several scenarios were given for every thickness and compressive strength combination. Each (t, f_c) pair was analyzed through MCS to determine its corresponding reliability index. This approach captures the combined effect of both parameters on structural reliability, enabling the ANN to learn complex nonlinear interactions. Given that MCS was performed for multiple (t, f_c) combinations, it was impractical to include all generated data points in ANN training (each MCS for (t, f_c) was 500,000 data points). Instead, a subset of scenarios was selected based on the following considerations: Only a few representative points were taken for failure cases to avoid redundancy while ensuring that the ANN was adequately trained to recognize failure conditions. In scenarios where all values in a given category failed (example: t=*0.2 m*), it was unnecessary to include every single case, as they all conveyed the same outcome. Instead, a subset of representative failure cases was selected to cover a range of failure conditions without overwhelming the dataset with repetitive information. The selection considered different levels of failure severity, ensuring the ANN could distinguish between cases far from meeting the reliability target and those near the transition zone. For transition cases, values were chosen to ensure coverage of intermediate reliability states. These cases are characterized by reliability indices that are either just below or slightly above the target value. By including scenarios that marginally fail to meet the reliability requirement and those that barely surpass it, the ANN gains exposure to cases where structural performance is uncertain or borderline. This is particularly important for capturing the sensitivity of the reliability index to changes in thickness and compressive strength, allowing the model to better distinguish between cases that are the threshold of failure and those that are marginally safe.

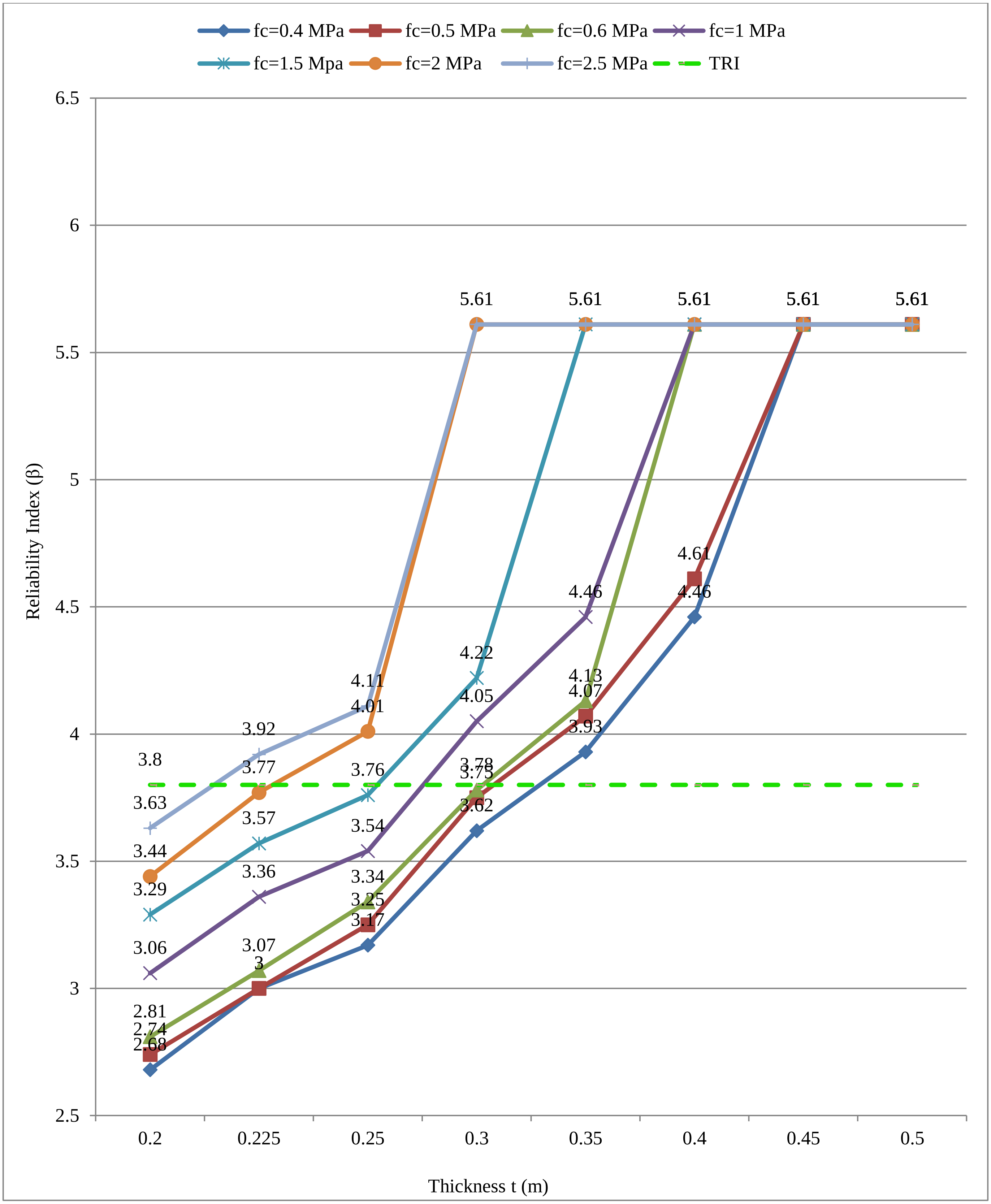

Fig. 4 Reliability index as a function of wall thickness for various assessed compressive strength. The plot illustrates how reliability changes with wall thickness, grouped by compressive strength values (TRI denotes the Target Reliability Index)

For success cases, two distinct categories were considered:

- Partial success cases, where the reliability index surpasses the target value but the probability of failure is not zero ($TRI = 3.8 < \beta < 5.61$). These cases represent structures that, while meeting the minimum reliability requirement, still carry a small probability of failure.
- Full success cases, where the probability of failure is effectively 0% ($\beta = 5.61$). These cases ensure that the ANN learns to recognize configurations that provide complete structural safety.

To maintain computational efficiency, rather than including all 500,000 iterations per scenario, a subset of 1639 data points was extracted from each selected scenario. This number provides sufficient training samples from each scenario while avoiding excessive computational costs. The selection of data for training the ANN was carefully designed to ensure that the model effectively learns the relationship between the key parameters and the reliability of rammed earth under wind pressure. Moreover, while the selection process was not based on a strict mathematical formula, care was taken to ensure a balanced dataset that prevents the ANN from being biased toward a particular reliability outcome. The ANN is expected to learn robust decision boundaries for predicting reliability indices across different structural configurations by including a well-distributed mix of failure, transition, and success cases.

Table 8 presents the input scenarios used for the ANN dataset, showing the wall thickness, compressive strength, and the associated reliability outcome (Failure or Success).

Data Preprocessing

Data preprocessing plays a crucial role in preparing the ANN model, particularly due to the differing scales of the input features [111]. In this case, using feature normalization and standardization helps ensure that machine learning models perform correctly while also improving the model's training efficiency and accuracy [111]. Normalization and standardisation are critical techniques when dealing with algorithms sensitive to input value ranges, such as SVMs and neural networks. Min-max normalization and z-score standardization are the most widely used [112].

Thus, to ensure consistent scaling of input features, min-max normalization was applied, transforming all variables to a range between 0 and 1 based on Equation 10 [113]:

$$X_N = \frac{X_i - X_{min}}{Xmin_{max}} \tag{10}$$

Where X_i is the original value of the data point before normalization, X_{min} and X_{max} Are the minimum and maximum values in the dataset, respectively, and X_N the result of the normalization of X_i, scaled to be between 0 and 1.

Network Architecture and Training Methodology

The ANN is implemented using a feed-forward backpropagation approach, with weight optimization performed using the Levenberg-Marquardt (LM) algorithm in MATLAB due to its robust neural network toolbox, which provides built-in functions for training, validating and testing neural networks.

Feed-forward neural networks are selected due to their widespread use in solving complex problems [114]. Their popularity stems from their ability to approximate nonlinear functions effectively, making them particularly suited for reliability analysis and regression tasks.

The backpropagation algorithm is employed as the learning rule, where the error signal-defined as the difference between the predicted and actual output- is propagated in reverse through the network to update the weights from the output to the input via the hidden layers [115].

This iterative process ensures the model progressively improves its predictive accuracy by adjusting the network parameters at each step [115].

The Levenberg-Marquardt (LM) algorithm is chosen for optimisation due to its suitability for nonlinear regression tasks. Initially developed in the early 1960s to solve nonlinear least square problems [116], LM is one of the most widely used optimization algorithms [117].

The dataset is split into 80% training, 10% validation and 10% testing subsets.

Hyperparameter Optimization

To determine the optimal ANN configuration, several hyperparameters were systematically varied.

Table 8. Selected Input Scenarios for ANN Modeling, Representing Both Failure and Success Outcomes Across Wall Thicknesses and Compressive Strengths

Thickness t (m)	Compressive Strength f_c (MPa)	State
0.2	0.4	Failure
0.2	0.5	Failure
0.225	0.5	Failure
0.25	0.6	Failure
0.25	1	Failure
0.3	0.6	Failure
0.3	1	Success
0.35	1	Success
0.4	1	Success
0.45	1.5	Success
0.45	2	Success
0.5	2.5	Success

- Activation function: Different transfer functions were tested, including the Sigmoid and Tangential Sigmoid Function (tansig), and the Rectified Linear Unit (ReLU) provided the best performance.
- Learning rate: A learning rate of 0.001 was found to
- offer the best balance between convergence speed and stability.
- Early stopping: Early stopping with patience of 6 epochs was applied to prevent overfitting.
- Regularization: A regularization parameter 0.01 was used after testing different values to improve generalisation and reduce overfitting during training.
- Number of hidden layers and neurons: The study varied the number of hidden layers from two to three to investigate their effect on the model's efficiency. The number of neurons per layer was extensively tested, and the final configurations are summarized in Table 9 for two hidden layers and Table 10 for three hidden layers.

The final MATLAB script, shown in Figure 5, illustrates the implementation of this procedure.

Performance Evaluation and Model Comparison

Two metrics were used to evaluate the performance of the various ANN configurations tested in this study: The Mean Squared Error (MSE) and the Coefficient of Determination (R^2). These metrics were calculated for each configuration to assess prediction accuracy and goodness of fit. The results are summarized in Table 9 and Table 10 for networks with two and three hidden layers, respectively. In addition, Figures 6 and Figure 7 visualize the performance of each configuration in terms of MSE and R^2, respectively, with each point representing a distinct ANN architecture. This graphical representation directly compares how different network structures perform for error minimization and predictive strength.

3.3.3. Cross-Validation and Model Robustness

Based on the results presented in Table 9, Table 10, Figure 6 and Figure 7, the ANN configuration that yielded the best performance was Net311 (architecture presented in Figure 8), which consists of three hidden layers, with the first layer containing 11 neurons, the second layer with 12 neurons, and the third layer with 13 neurons.

```
% Loading the dataset
input = inptest;  % Input features
target = targtest; % Target labels
% Creating and configurating the network
% Feedforward neural network with two hidden layers, using Levenberg-Marquardt as a training algorithm:
% the first layer has 1 neuron, and the second has 2 neurons.
nettest = feedforwardnet( [1 2], 'trainlm');
net.performParam.regularization = 0.01;  % % Applying L2 regularization to reduce overfitting
% Setting ReLU activation function for the hidden layers
net.layers{1}.transferFcn='poslin';
net.layers{2}.transferFcn='poslin';
% Setting training parameters
net.trainParam.lr = 0.001; % Learning rate
net.trainParam.epochs = 2000; % Max epochs
net.trainParam.goal = 1e-6; % MSE goal
net.trainParam.max_fail = 6; % Early stopping (6 validation failures)
% Setting Mean Squared Error (MSE) as the loss function
net.performFcn = 'mse';
% Setting data division
net.divideFcn = 'dividerand';
net.divideParam.trainRatio = 0.8;  % 80% of the dataset for training
net.divideParam.valRatio = 0.1;  % 10% of the dataset for validation
net.divideParam.testRatio = 0.1;  %10% of the dataset for testing
% Training the network
 [nettest, tr] = train(nettest, input, target);
% Predicting outputs using the trained network
y_pred = nettest(input);
% Computing Mean Squared Error (MSE) to evaluate prediction accuracy
mse_value = perform(nettest, target, y_pred);
fprintf('Mean Squared Error (MSE): %.6f\n', mse_value);
% Computing R² (Coefficient of Determination)
SStot = sum((target - mean(target)).^2);  % Total sum of squares
SSres = sum((target - y_pred).^2);       % Residual sum of squares
R_squared = 1 - (SSres / SStot);         % Compute R²
fprintf('Coefficient of Determination (R²): %.6f\n', R_squared);
```

Fig. 5 MATLAB Script for ANN Implementation, Showing Key Hyperparameter Settings, Training Process, and Performance Metrics

Although this model demonstrates the highest performance among the configurations tested, assessing its stability after training remains crucial. This step ensures that the model effectively learns the underlying data patterns without overfitting and can maintain reliable predictive accuracy when applied to independent, previously unseen data during deployment [118].

In this context, cross-validation is used as a resampling technique of the most widely adopted approaches for evaluating machine learning models to provide an unbiased estimate of model performance on unseen data [119, 120].

Table 9. ANN configurations with two hidden layers and corresponding performance metrics

Hidden Layers	Number of neurons	ID	MSE	R^2
Two	[1 2]*	Net21	0.028135	0.824212
	[2 3]	Net22	0.023788	0.851372
	[3 4]	Net23	0.023836	0.851074
	[4 5]	Net24	0.023894	0.850709
	[5 6]	Net25	0.02467	0.845864
	[6 7]	Net26	0.024008	0.850002
	[7 8]	Net27	0.0239	0.850672
	[8 9]	Net28	0.02431	0.848112
	[9 10]	Net29	0.023929	0.850495
	[10 11]	Net210	0.025002	0.84790
	[11 12]	Net211	0.023531	0.852983

* [i j] Denotes the number of neurons in the first (i) and second (j) hidden layers, respectively

Specifically, k-fold cross-validation with k=10 is performed in this study, as it is considered a sensible choice that provides an almost unbiased estimate of prediction error [120]. K-fold cross-validation works by splitting the dataset into k random subsets. Each subset is used as the validation set once while the other k-1 subsets form the training set, and this cycle repeats k times [119].

Table 11 presents the results of the 10-fold cross-validation, including the MSE and the R^2 for each fold, along with the mean and standard deviation values for both metrics. The MATLAB script used to implement this cross-validation procedure is shown in Figure 9.

Table 10. ANN configurations with three hidden layers and corresponding performance metrics

Hidden Layers	Number of neurons	ID	MSE	R^2
Three	[1 2 3]*	Net31	0.028646	0.821025
	[2 3 4]	Net32	0.027832	0.826107
	[3 4 5]	Net33	0.023494	0.853208
	[4 5 6]	Net34	0.023891	0.850734
	[5 6 7]	Net35	0.02396	0.850298
	[6 7 8]	Net36	0.024204	0.848776
	[7 8 9]	Net37	0.023518	0.853062
	[8 9 10]	Net38	0.023583	0.852657
	[9 10 11]	Net39	0.024023	0.849904
	[10 11 12]	Net310	0.024966	0.844016
	[11 12 13]	Net311	0.023462	0.853408
	[12 13 14]	Net312	0.023753	0.851594
	[13 14 15]	Net313	0.02451	0.846866

* [i j k] Denotes the number of neurons in the first (i), second (j) and third (k) hidden layers, respectively

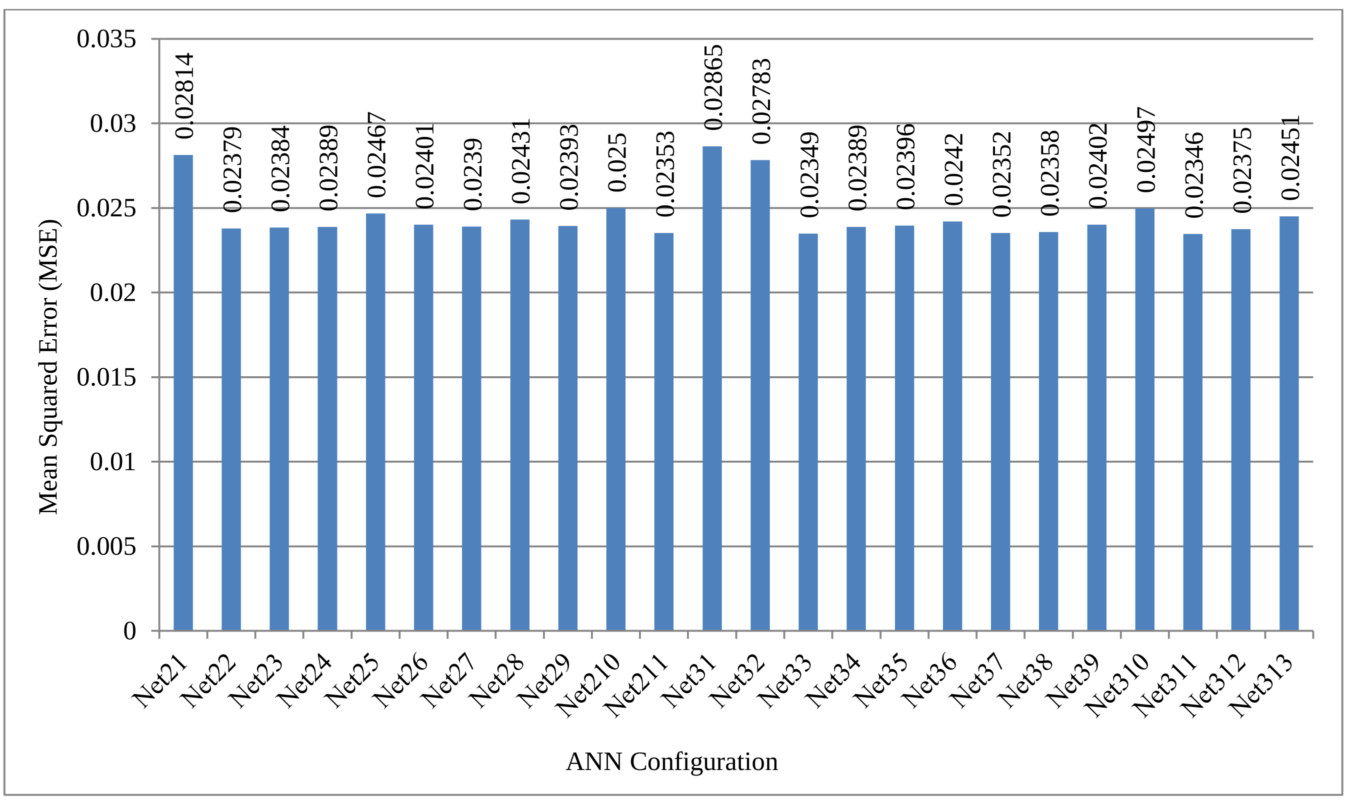

Fig. 6 Mean Squared Error (MSE) across different ANN configurations, highlighting model performance sensitivity to architecture variations

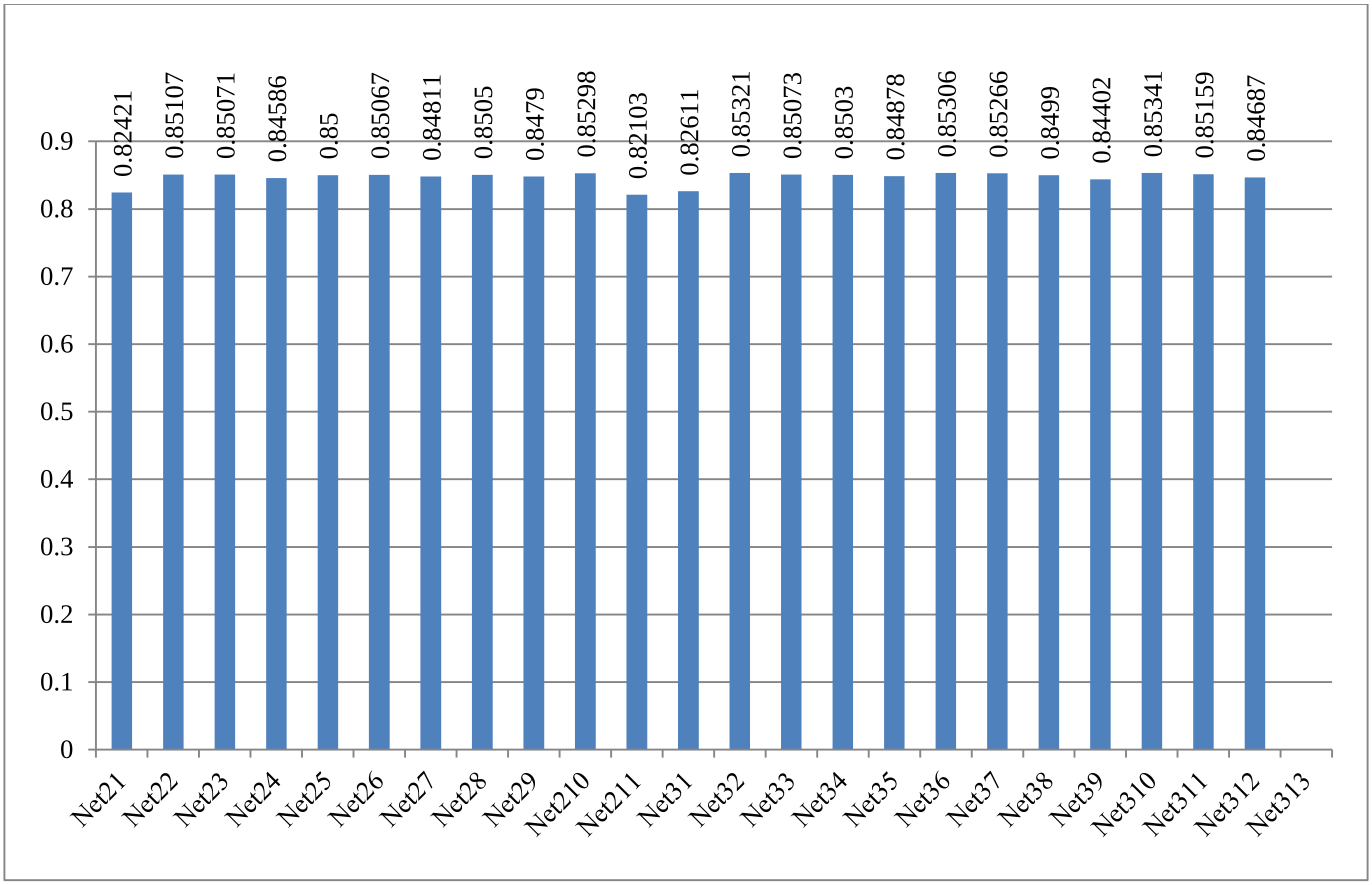

Fig. 7 Coefficient of determination (R^2) across ANN configurations, indicating the predictive accuracy of each model architecture

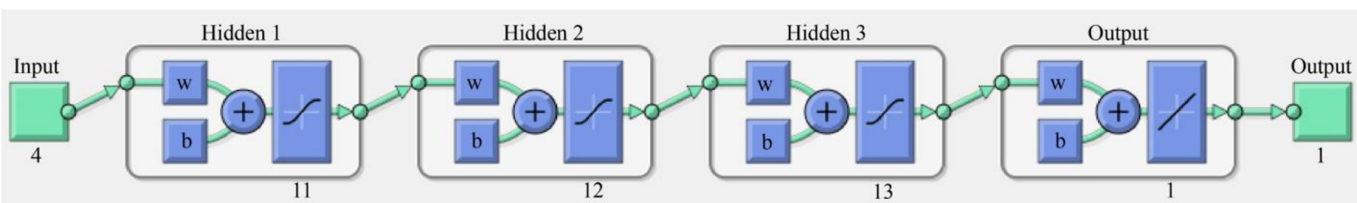

Fig. 8 Architecture of the best-performing neural network during training (net311), highlighting the three hidden layers with 11, 12 and 13 neurons respectively

Table 11. 10-Fold Cross-Validation Results: MSE and R^2 per Fold with Corresponding Mean and Standard Deviation

	MSE	R^2
Fold 1	0.028644	0.84603
Fold 2	0.027158	0.863122
Fold 3	0.037357	0.790097
Fold 4	0.03205	0.825052
Fold 5	0.03568	0.810011
Fold 6	0.033048	0.796914
Fold 7	0.035155	0.80964
Fold 8	0.02721	0.841083
Fold 9	0.034457	0.807754
Fold 10	0.030231	0.804821
Mean Value	0.032099	0.819452
Standard Deviation	0.003652	0.023614

```
k = 10; % Defining number of folds for k-fold cross-validation
N = size(inptest, 2); % Getting the number of samples in the dataset
cv = cvpartition(N, 'KFold', k); % Creating cross-validation partition with k folds
% Initializing arrays to store MSE and R² values
mse_values = zeros(k, 1);
r2_values = zeros(k, 1);

for i = 1:k
    % Extracting training and testing indices for the current fold
    trainIdx = training(cv, i);
    testIdx = test(cv, i);

    % Creating training and testing input/target sets for this fold
    inTrain = inptest(:, trainIdx);
    targTrain = targtest(:, trainIdx);

    inTest = inptest(:, testIdx);
    targTest = targtest(:, testIdx);

    % Initializing and training the feedforward neural network
    net = feedforwardnet( [1 2], 'trainlm'); % Example architecture
    net.performParam.regularization = 0.01;  % Applying L2 regularization
    net = train(net, inTrain, targTrain);

    % Predicting and evaluating performance
    y_pred = net(inTest);

    % Calculating Mean Squared Error (MSE)
    mse_value = perform(net, targTest, y_pred);
    mse_values(i) = mse_value;  % Storing MSE for the current fold

    % Calculating R² (coefficient of determination)
    ss_total = sum((targTest - mean(targTest)).^2);  % Total sum of squares
    ss_residual = sum((targTest - y_pred).^2);  % Residual sum of squares
    r2_value = 1 - (ss_residual / ss_total);  % R² formula
    r2_values(i) = r2_value;  % Store R² for the current fold

    % Displaying results for the current fold
    fprintf('Fold %d - MSE: %.6f, R²: %.6f\n', i, mse_value, r2_value);
end

% Calculating the mean and standard deviation of MSE and R²
mean_mse = mean(mse_values);
std_mse = std(mse_values);
mean_r2 = mean(r2_values);
std_r2 = std(r2_values);
% Displaying average performance metrics across all fold
fprintf('\nOverall Performance:\n');
fprintf('Mean MSE: %.6f, Std MSE: %.6f\n', mean_mse, std_mse);
fprintf('Mean R²: %.6f, Std R²: %.6f\n', mean_r2, std_r2);
```

Fig. 9 MATLAB script for 10-fold cross-validation showing data splitting, network training, and performance evaluation using MSe and R^2

4. Discussion

4.1. Monte Carlo Simulation

Based on the results illustrated in Figure 4, an increase in wall thickness and compressive strength leads to higher reliability index values. The behavior across different thicknesses can be summarized as follows:

- t = 0.20 m: The target reliability index is not reached for any of the compressive strengths evaluated (up to 2.5 MPa), indicating that this thickness requires higher compressive strength values than those tested. Therefore, it is not recommended under the conditions of this study.
- t = 0.225 m: The target reliability index is just barely met at $f_c = 2\,MPa$ and exceeded at $f_c = 2.5\,MPa$. This makes it a borderline option, suitable only when high compressive strength is ensured.
- t = 0.25 m: The target reliability index is achieved starting from $f_c = 2\,MPa$, indicating better performance and reliability.
- t = 0.30 m: The reliability index surpasses the target reliability index for all compressive strengths starting from 1 MPa, showing a robust and safe configuration.
- t = 0.35 m and above: The target reliability index is consistently met and exceeded for all evaluated compressive strength values, making this the safest and most reliable choice within the tested range.

In conclusion, a minimum wall thickness of 0.35 m is recommended to ensure structural reliability without depending on extremely high compressive strength. Conversely, thinner walls such as 0.20 m are not advisable unless higher compressive strengths (beyond 2.5 MPa) can be guaranteed.

To clarify these findings, Table 12 summarizes the minimum compressive strength values required to reach the target reliability index for each wall thickness evaluated in the context of this study, which can serve as a guide to optimize material use while maintaining structural reliability. Additionally, the computed 95% confidence intervals for the probability of failure values are consistently narrow across all compressive strength and wall thickness combinations.

This narrowness indicates high statistical confidence in the simulation outcomes, reflecting the stability of the MCS due to the large number of iterations (500,000). For instance, for a probability of failure as high as 0.3694, the interval is only ±0.0013, while even for rare failure probabilities such as 0.000001, the interval remains tightly bound between approximately 1×10^{-7} and 9.6×10^{-6}.

This consistency suggests that the failure probabilities are well-converged and the simulation results are reliable. Therefore, these confidence intervals reinforce the credibility of the structural reliability estimates derived from the MCS.

4.2. Artificial Neural Networks and Cross-Validation

As shown in the results, after conducting MCS, ANN was performed to develop a model that can predict the reliability index of URE under wind pressure in the scope of recommendations existing in current technical documents. The results of ANN in both Table 9 and Table 10 and their representation in Figure 6 and Figure 7 showed that Net311 represented the best results based on the metrics studied (MSE and R^2).

Furthermore, the k-fold cross-validation method was used to validate the model. The ANN model demonstrated a strong predictive capability during training, with $R^2=0.853408$, meaning the model explains 85% of the data and $MSE=0.023462$, close to 0. This indicates that the network successfully captured the underlying relationships between the input and output variables.

The performance plot (Figure 10) shows that the best validation performance was achieved at epoch 10, beyond which the validation error increased while the training error continued to decrease. This suggests that early stopping was effectively applied to prevent overfitting, ensuring good generalization.

Furthermore, the regression plots for training (Figure 11), validation, and test sets all reveal strong linear relationships with correlation coefficients above 0.9. The closeness of predicted outputs to actual targets across all datasets confirms the ANN model's ability to predict the reliability index reliably. These results validate the robustness and predictive power of the selected ANN configuration. The cross-validation results ($R^2=0.819452$ and $MSE=0.032099$) showed a slight reduction in performance compared to the training phase.

This decline reflects the natural challenge of generalizing beyond the data the model was initially trained on. Notably, the relatively low value of standard deviation for both MSE and R^2 (respectively 0.03652 and 0.023614) indicates the consistency of the performance across all folds and suggests that the model is stable and not only sensitive to the particular data subset it is trained (Table 11).

Moreover, the R^2 values remained relatively high throughout cross-validation (Table 11), indicating that the model consistently explained a significant proportion of the variance (more than 79%) in the output variable, even across different validation sets. The model error remained within a tight range, confirming its predictive reliability.

Overall, the cross-validation process reinforces the quality of the chosen ANN configuration. The slight discrepancy between training and validation performance is a normal and desirable outcome, confirming that the model is learning the general patterns in the data rather than simply memorizing them. This provides strong support for the suitability of the final model architecture.

Table 12. Recommended Minimum Compressive Strengths to Achieve Target Reliability Index for Varying Wall Thicknesses, Based on Simulation Results

	Values of thickness assessed (m)							
	0.2	0.225	0.25	0.3	0.35	0.4	0.45	0.5
Minimal compressive strength recommended (MPa)	-*	2.5	2	1	0.5	0.5	0.5	0.5

*This value is not recommended in the context of this study

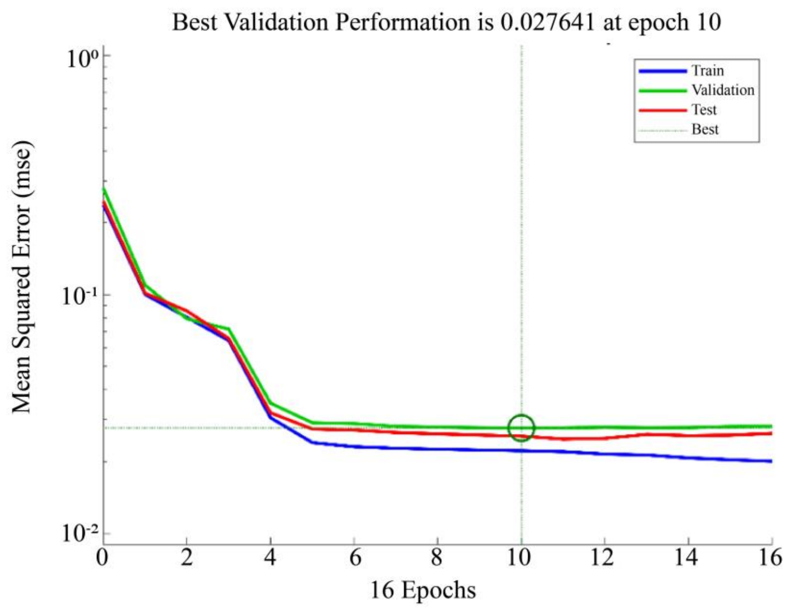

Fig. 10 Model performance evaluation based on Mean Squared Error (MSE) during training, showing best validation performance at epoch 10

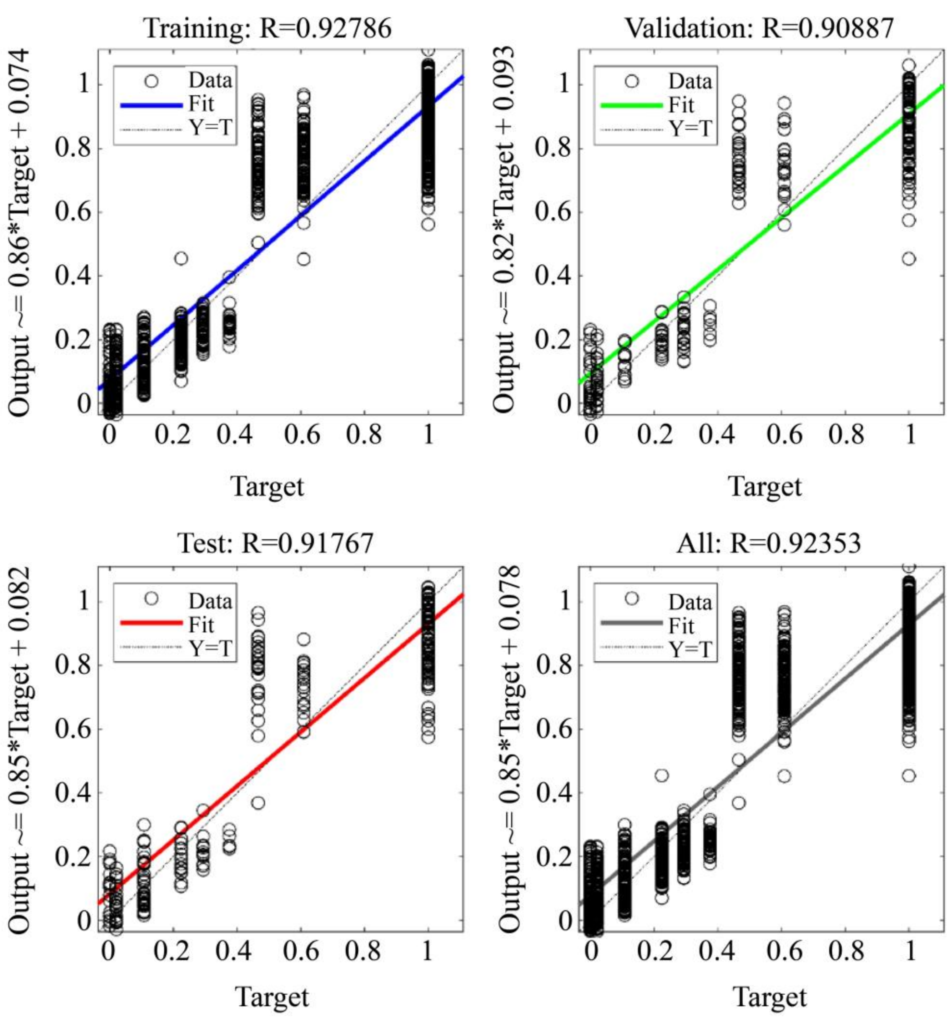

Fig. 11 Regression performance of the ANN model across training, validation, and test sets

5. Conclusion

This study applied MCS and ANN to assess the reliability of URE structures under lateral wind forces. The MCS was conducted to generate a robust dataset for training the ANN model while also performing a reliability analysis of the structure's performance under varying conditions. The analysis was based on a limit state function derived from the elastic analysis in the study by Ciandio and Augarde [18] and the French Snow and Wind Load Regulations (NV65) [33]. The simulation included many iterations to incorporate randomness in key variables such as compressive strength, wall thickness, wind speed, and other relevant factors. To enhance the credibility of the probabilistic outcomes, 95% confidence intervals were calculated for each estimated probability of failure using the Wilson score method; the consistently narrow bounds confirmed the statistical stability of the results. The MCS results indicated that a wall thickness of 0.2 m was insufficient for the range of compressive strengths assessed, with the minimum thickness of 0.35 m ensuring safety across all compressive strength values considered. These findings are crucial for establishing practical design recommendations for URE under wind load conditions.

The ANN model, developed using the dataset generated from the MCS, showed strong performance in predicting the structural reliability of URE under lateral wind forces. The model demonstrated good convergence with an MSE of 0.023 and an R^2 value of 0.853, indicating its ability to learn the complex relationships in the data. Further evaluation using 10-fold cross-validation confirmed the robustness and generalizability of the model, with only a slight increase in MSE and a modest reduction in R^2, demonstrating the model's stability and accuracy across different data subsets.

The findings of this study offer practical guidance for the design of URE structures under wind loads. The probabilistic analysis provides minimum compressive strength requirements for different wall thicknesses, allowing engineers to make informed design decisions with a quantifiable safety margin. An ANN model also enables rapid reliability assessment without requiring full-scale simulations, supporting efficient design iteration. Incorporating these results into design guidelines or performance-based codes could improve URE's structural safety and acceptance in modern construction.

In this study, the limit state function was primarily based on the elastic analysis outlined in the work of Ciancio and Augarde [18], along with the NV65 [33] regulations. However, alternative methods for developing the limit state function could provide additional insights, particularly by directly incorporating tensile strength values where experimental data is available. Expanding the analysis to consider a broader range of wall dimensions, including length, height, and span variations between load-bearing walls, could further enhance the understanding of URE's structural performance under lateral wind forces.

Future research could also consider a broader set of compressive strengths and thickness values to extend the applicability of the findings to different structural configurations. Moreover, testing different ANN architectures and exploring alternative hyperparameter optimization methods may improve the model's predictive accuracy. Finally, considering the combined impact of wind forces and seismic loads on URE structures and validating the model with experimental data would provide a more comprehensive understanding of the performance and reliability of URE under various loading conditions.

Funding Statement

This research was supported by the National Centre for Scientific and Technical Research (CNRST), Morocco, under the Excellence Research Fellowship Program.

Ethical Approval

This study did not involve human participants, animals, or protected heritage structures and, therefore, did not require ethical approval.

References

[1] Antoine Pelé-Peltier et al., "A Similitude Relation to Assessing the Compressive Strength of Rammed Earth from Scale-Down Samples," *Case Studies in Construction Matearials*, vol. 16, pp. 1-14, 2022. [CrossRef] [Google Scholar] [Publisher Link]

[2] Mostafa Shaaban, "Sustainability of Excavation Soil and Red Brick Waste in Rammed Earth," *Civil Engineering and Architecture*, vol. 9, no. 3, pp. 789-798, 2021. [CrossRef] [Google Scholar] [Publisher Link]

[3] Fernando Ávila, Esther Puertas, and Rafael Gallego, "Characterization of the Mechanical and Physical Properties of Unstabilized Rammed Earth: A Review," *Construction and Building Materials*, vol. 270, 2021. [CrossRef] [Google Scholar] [Publisher Link]

[4] Mohamed Gomaa et al, "Automation in Rammed Earth Construction for Industry 4.0: Precedent Work, Current Progress and Future Prospect," *Journal of Cleaner Production*, vol. 398, pp. 1-14, 2023. [CrossRef] [Google Scholar] [Publisher Link]

[5] Daniela Ciancio, Paul Jaquin, and Peter Walker, "Advances on the Assessment of Soil Suitability for Rammed Earth," *Construction and Building Materials*, vol. 42, pp. 40-47, 2013. [CrossRef] [Google Scholar] [Publisher Link]

[6] Quoc-Bao Bui et al., "Compression Behaviour of Non-Industrial Materials in Civil Engineering by Three Scale Experiments: The Case of Rammed Earth," *Materials and Structures*, vol. 42, pp. 1101-1116, 2009. [CrossRef] [Google Scholar] [Publisher Link]

[7] David Thompson, Charles Augarde, and Juan Pablo Osorio, "A Review of Current Construction Guidelines to Inform the Design of Rammed Earth Houses in Seismically Active Zones," *Journal of Building Engineering*, vol. 54, pp. 1-15, 2022. [CrossRef] [Google Scholar] [Publisher Link]

[8] C.S. Costa, F. Rocha, and A.L. Velosa, "Sustainability in Earthen Heritage Conservation," *Geological Society, London, Special Publications*, vol. 416, pp. 91-100, 2016. [CrossRef] [Google Scholar] [Publisher Link]

[9] Julian Keable, and Rowland Keable, *Rammed Earth Structures*, Practical Action Publishing, pp. 1-128, 2011. [Google Scholar] [Publisher Link]

[10] Lorenzo Miccoli, Urs Müller, and Patrick Fontana, "Mechanical Behaviour of Earthen Materials: A Comparison between Earth Block Masonry, Rammed Earth and Cob," *Construction and Building Materials*, vol. 61, pp. 327-339, 2014. [CrossRef] [Google Scholar] [Publisher Link]

[11] Abdelhakim El Bourki, Ahmed Koutous, and Elmokhtar Hilali, "Date Palm Fiber-Reinforcement Impact on Rammed Earth Mechanical Behavior," *Construction and Building Materials*, vol. 461, 2025. [CrossRef] [Google Scholar] [Publisher Link]

[12] Aryan Baibordy, Mohammad Yekrangnia, and Saeed Ghaffarpour Jahromi, "A Comprehensive Study on the Mechanical Properties of Natural Fiber Reinforced Stabilized Rammed Earth Using Experimental and Data-Driven Fuzzy Logic-Based Analysis," *Cleaner Materials*, vol. 15, pp. 1-31, 2025. [CrossRef] [Google Scholar] [Publisher Link]

[13] Pengfei Xu et al., "Study on Hydrothermal Migration and Interface Cracking Mechanisms of Supporting Reinforcing Bodies in the Root Erosion Zones of Rammed Earth Sites in Arid Regions," *Construction and Building Materials*, vol. 457, 2024. [CrossRef] [Google Scholar] [Publisher Link]

[14] Carene Umubyeyi et al., "Durability of Unstabilized Rammed Earth in Temperate Climates: A Long Term Study," *Construction and Building Materials*, vol. 409, pp. 1-29, 2023. [CrossRef] [Google Scholar] [Publisher Link]

[15] Tiegang Zhou et al., "Investigation of Intralayer and Interlayer Shear Properties of Stabilized Rammed Earth by Direct Shear Tests," *Construction and Building Materials*, vol. 367, 2023. [CrossRef] [Google Scholar] [Publisher Link]

[16] Qiangqiang Pei et al, "Study on Numerical Simulation Analysis Methods of Multi-layer Discontinuous Rammed Earth Structure," *Physics and Chemistry of the Earth, Parts A/B/C*, vol. 140, 2025. [CrossRef] [Google Scholar] [Publisher Link]

[17] Eoghan Healy, and Juan Pablo Osorio, "Modelling the Behaviour of Rammed Earth Walls Using Finite Element Analysis," *School of Transport and Civil Engineering: Proceedings of the conference Civil Engineering Research in Ireland 2024 Conference*, Ireland, pp. 184-189, 2024. [CrossRef] [Google Scholar] [Publisher Link]

[18] D. Ciancio, and C. Augarde, "Capacity of Unreinforced Rammed Earth Walls Subject to Lateral Wind Force: Elastic Analysis Versus Ultimate Strength Analysis," *Materials and Structures*, vol. 46, pp. 1569-1585, 2013. [CrossRef] [Google Scholar] [Publisher Link]

[19] Yi Luo et al., "Degradation of Rammed Earth under Wind-Driven Rain: The Case of Fujian Tulou, China," *Construction and Building Materials*, vol. 261, 2020. [CrossRef] [Google Scholar] [Publisher Link]

[20] Ehsan Kianfar, and Vahab Toufigh, "Reliability Analysis of Rammed Earth Structures," *Construction and Building Materials*, vol. 127, pp. 884-895, 2016. [CrossRef] [Google Scholar] [Publisher Link]

[21] Hubert Anysz, and Piotr Narloch, "Designing the Composition of Cement Stabilized Rammed Earth Using Artificial Neural Networks," *Materials*, vol. 12, no. 9, pp. 1-27, 2019. [CrossRef] [Google Scholar] [Publisher Link]

[22] Yassir Mubarak Hussein Mustafa et al., "Analysis of Unconfined Compressive Strength of Rammed Earth Mixes Based on Artificial Neural Network and Statistical Analysis," *Materials*, vol. 15, no. 24, pp. 1-24, 2022. [CrossRef] [Google Scholar] [Publisher Link]

[23] Hubert Anysz et al., "Feature Importance of Stabilised Rammed Earth Components Affecting the Compressive Strength Calculated with Explainable Artificial Intelligence Tools," *Materials*, vol. 13, no. 10, pp. 1-20, 2020. [CrossRef] [Google Scholar] [Publisher Link]

[24] Piotr Narloch et al., "Predicting Compressive Strength of Cement-Stabilized Rammed Earth Based on SEM Images Using Computer Vision and Deep Learning," *Applied Sciences*, vol. 9, no. 23, pp. 1-14, 2019. [CrossRef] [Google Scholar] [Publisher Link]

[25] Wafaa Wardah et al., "Protein Secondary Structure Prediction Using Neural Networks and Deep Learning: A Review," *Computational Biology and Chemistry*, vol. 81, pp. 1-8, 2019. [CrossRef] [Google Scholar] [Publisher Link]

[26] Maria Idália Gomes, Teresa Diaz Gonçalves, and Paulina Faria, "Unstabilized Rammed Earth: Characterization of Material Collected from Old Constructions in South Portugal and Comparison to Normative Requirements," *International Journal of Architectural Heritage*, vol. 8, no. 2, pp. 185-212, 2014. [CrossRef] [Google Scholar] [Publisher Link]

[27] Keith Zawistowski, Marie Zawistowski, and Thierry Joffroy, "Evolving Vernacular: Reinventing Rammed Earth in the Context of Twenty-First Century Seismic Regulation," *Technology|Architecture + Design*, vol. 4, no. 2, pp. 158-165, 2020. [CrossRef] [Google Scholar] [Publisher Link]

[28] Abdellah Mellaikhafi et al., "Characterization of Different Earthen Construction Materials in Oasis of South-eastern Morocco (Errachidia Province)," *Case Studies in Construction Materials*, vol. 14, pp. 1-18, 2021. [CrossRef] [Google Scholar] [Publisher Link]

[29] Juan C. Reyes et al., "Shear Behavior of Adobe and Rammed Earth Walls of Heritage Structures," *Engineering Structures*, vol. 174, pp. 526-537, 2018. [CrossRef] [Google Scholar] [Publisher Link]

[30] The Moroccan Seismic Regulation for Earth Constructions (RPC Terre 2011), 2011.

[31] Fabio Matta, Mabel C. Cuéllar-Azcárate, and Enrico Garbin, "Earthen Masonry Dwelling Structures for Extreme Wind Loads," *Engineering Structures*, vol. 83, pp. 163-175, 2015. [CrossRef] [Google Scholar] [Publisher Link]
[32] Vasilios Maniatidis, and Peter Walker, *A Review of Rammed Earth Construction*, Natural Building Technology Group, pp. 1-109, 2003. [Google Scholar] [Publisher Link]
[33] NV65 Rules Defining the Effects of Snow and Wind on Buildings and Annexes, 2024. [Online]. Available: http://www.icab.eu/guide/nv65/
[34] Yong Bai, and Wei-Liang Jin, *Random Variables and Uncertainty Analysis*, Marine Structural Design, Elsevier Science, pp. 615-625, 2015. [Google Scholar] [Publisher Link]
[35] H. Gulvanessian, Jean-Armand Calgaro, and Milan Holický, *Designer's Guide to EN 1990: Eurocode: Basis of Structural Design*, Thomas Telford, pp. 1-192, 2002. [Google Scholar] [Publisher Link]
[36] Mariano Angelo Zanini, and Lorenzo Hofer, "Center and Characteristic Seismic Reliability as New Indexes for Accounting Uncertainties in Seismic Reliability Analysis," *Soil Dynamics and Earthquake Engineering*, vol. 123, pp. 110-123, 2019. [CrossRef] [Google Scholar] [Publisher Link]
[37] Haiyang Song, and Jian Zhang, "Structural Reliability Analysis Based on Interval Analysis Method in Statistical Energy Analysis Framework," *Mechanics Research Communications*, vol. 117, 2021. [CrossRef] [Google Scholar] [Publisher Link]
[38] Ross B. Corotis, "An Overview of Uncertainty Concepts Related to Mechanical and Civil Engineering," *ASCE-ASME Journal of Risk and Uncertainty in Engineering Systems, Part B: Mechanical Engineering*, vol. 1, no. 4, pp. 1-12, 2015. [CrossRef] [Google Scholar] [Publisher Link]
[39] Changqi Luo et al., "An Enhanced Uniform Simulation Approach Coupled with SVR for Efficient Structural Reliability Analysis," *Reliability Engineering & System Safety*, vol. 237, pp. 2023. [CrossRef] [Google Scholar] [Publisher Link]
[40] Chao Dang et al., "Structural Reliability Analysis by Line Sampling: A Bayesian Active Learning Treatment," *Structural Safety*, vol. 104, pp. 1-35, 2023. [CrossRef] [Google Scholar] [Publisher Link]
[41] C.G. Bucher, and U. Bourgund, "A Fast and Efficient Response Surface Approach for Structural Reliability Problems," *Structural Safety*, vol. 7, no. 1, pp. 57-66, 1990. [CrossRef] [Google Scholar] [Publisher Link]
[42] H. Xu, and S. Rahman, "Decomposition Methods for Structural Reliability Analysis," *Probabilistic Engineering Mechanics*, vol. 20, no. 3, pp. 239-250, 2005. [CrossRef] [Google Scholar] [Publisher Link]
[43] Jun Xu, and Shengyang, "An Efficient Approach for High-Dimensional Structural Reliability Analysis," *Mechanical Systems and Signal Processing*, vol. 122, pp. 152-170, 2019. [CrossRef] [Google Scholar] [Publisher Link]
[44] Chao Dang et al., "Parallel Adaptive Bayesian Quadrature for Rare Event Estimation," *Reliability Engineering & System Safety*, vol. 225, pp. 1-30, 2022. [CrossRef] [Google Scholar] [Publisher Link]
[45] Yuming Zhang, and Juan Ma et al., "An Improved Sequential Importance Sampling Method for Structural Reliability Analysis of High Dimensional Problems," *Structures*, vol. 68, 2024. [CrossRef] [Google Scholar] [Publisher Link]
[46] Achintya Haldar, and Sankaran Mahadevan, *First-Order and Second-Order Reliability Methods*, Probabilistic Structural Mechanics Handbook, Springer, Boston, MA, pp. 27-52, 1995. [CrossRef] [Google Scholar] [Publisher Link]
[47] Rui Teixeira, Maria Nogal, and Alan O'Connor, "Adaptive Approaches in Metamodel-Based Reliability Analysis: A Review," *Structural Safety*, vol. 89, pp. 1-18, 2021. [CrossRef] [Google Scholar] [Publisher Link]
[48] Nicholas Metropolis, and S. Ulam, "The Monte Carlo Method," *Journal of the American Statistical Association*, vol. 44, no. 247, pp. 335-341, 1949. [Google Scholar] [Publisher Link]
[49] Sajad Saraygord Afshari et al., "Machine Learning-Based Methods in Structural Reliability Analysis: A Review," *Reliability Engineering & System Safety*, vol. 219, 2022. [CrossRef] [Google Scholar] [Publisher Link]
[50] Naser Cheraghi, Mahmoud Miri, and Mohsen Rashki, "An Adaptive Artificial Neural Network for Reliability Analyses of Complex Engineering Systems," *Applied Soft Computing*, vol. 132, 2023. [CrossRef] [Google Scholar] [Publisher Link]
[51] Danial Dehghan-Souraki et al., "Optimizing Sediment Transport Models by Using the Monte Carlo Simulation and Deep Neural Network (Dnn): A Case Study of the Riba-Roja Reservoir," *Environmental Modelling & Software*, vol. 175, pp. 1-15, 2024. [CrossRef] [Google Scholar] [Publisher Link]
[52] Roshanak Rezaei Kalantary, Gelavizh Barzegar, and Sahand Jorfi, "Monitoring of Pesticides in Surface Water, Pesticides Removal Efficiency in Drinking Water Treatment Plant and Potential Health Risk to Consumers Using Monte Carlo Simulation in Behbahan City, Iran," *Chemosphere*, vol. 286, 2022. [CrossRef] [Google Scholar] [Publisher Link]
[53] Xinyu Xia et al., "Analysis of Carbon Peak Achievement at the Provincial Level in China: Construction of Ensemble Prediction Models and Monte Carlo Simulation," *Sustainable Production and Consumption*, vol. 50, pp. 445-461, 2024. [CrossRef] [Google Scholar] [Publisher Link]
[54] Álvaro Rodríguez-Rivas, and Mariano López de Haro, "Liquid-vapor Equilibrium and Critical Point of Parabolic-well Fluids of Variable width Derived from Gibbs Ensemble Monte Carlo Simulation," *Journal of Molecular Liquids*, vol. 386, pp. 1-5, 2023. [CrossRef] [Google Scholar] [Publisher Link]

[55] Mohamed Ait Tamerd et al., "Investigation of the Magnetoelectric Properties of Bi0.9La0.1Fe0.9Mn0.1O3/La0.8Sr0.2MnO3 Bilayer: Monte Carlo Simulation," *Physica B: Condensed Matter*, vol. 667, pp. 1-19, 2023. [CrossRef] [Google Scholar] [Publisher Link]

[56] Weijie Cui, Yuan Tian, and Jianrong Dai, "Novel Multileaf Collimator Designs with Tongues and Grooves in Leaf End and Monte Carlo Simulations," *Medical Dosimetry*, vol. 49, no. 3, pp. 254-262, 2024. [CrossRef] [Google Scholar] [Publisher Link]

[57] Yuhan Jing et al., "Monte Carlo Simulation of Water Diffusion through Cardiac Tissue Models," *Medical Engineering & Physics*, vol. 120, pp. 1-43, 2023. [CrossRef] [Google Scholar] [Publisher Link]

[58] Mehdi Hassanpour et al., "Monte Carlo Simulation of Spallation Fragments Cross-Sections and Yield for Proton Beam Interaction with 222Rn," *Alexandria Engineering Journal*, vol. 87, pp. 652-661, 2024. [CrossRef] [Google Scholar] [Publisher Link]

[59] Keyao Song, Fabrizio Scarpa, and Mark Schenk, "Manufacturing Sensitivity Study of Tensegrity Structures Using Monte Carlo Simulations," *International Journal of Solids and Structures*, vol. 298, pp. 1-17, 2024. [CrossRef] [Google Scholar] [Publisher Link]

[60] Charalampos G. Templalexis, and Georgios T. Xanthopoulos, "Monte Carlo Simulation and Sensitivity Analysis of the Michaëlis-Menten Kinetic Equation for the CO2 Inhibition Response to O2 Consumption During Storage of Fresh Produce," *Biosystems Engineering*, vol. 232, pp. 129-140, 2023. [CrossRef] [Google Scholar] [Publisher Link]

[61] Łukasz Smakosz, Cezary Szydłowski, and Jarosław Górski, "Monte Carlo Simulations of the Fracture Resistance of an Asphalt Pavement Layer," *Construction and Building Materials*, vol. 452, 2024. [CrossRef] [Google Scholar] [Publisher Link]

[62] Liang Chen et al, "Efficient Algorithm for Elastic Buckling of Corroded I-Section Steel Members with Monte Carlo Simulation," *Thin-Walled Structures*, vol. 175, 2022. [CrossRef] [Google Scholar] [Publisher Link]

[63] Monica Susanne Löfman, and Leena Katariina Korkiala-Tanttu, "Reliability Analysis of Consolidation Settlement in Clay Subsoil Using FOSM and Monte Carlo Simulation," *Transportation Geotechnics*, vol. 30, pp. 1-11, 2021. [CrossRef] [Google Scholar] [Publisher Link]

[64] S. Lek, and Y.S. Park, *Artificial Neural Networks*, Encyclopedia of Ecology, Academic Press, pp. 237-245, 2008. [CrossRef] [Google Scholar] [Publisher Link]

[65] Warren S. McCulloch, and Walter Pitts, "A Logical Calculus of the Ideas Immanent in Nervous Activity," *The Bulletin of Mathematical Biophysics*, vol. 5, pp. 115-133, 1943. [CrossRef] [Google Scholar] [Publisher Link]

[66] F. Rosenblatt, "The Perceptron: A Probabilistic Model for Information Storage and Organization in the Brain," *Psychological Review*, vol. 65, no. 6, pp. 386-408, 1958. [CrossRef] [Google Scholar] [Publisher Link]

[67] Steven Walczak, and Narciso Cerpa, *Artificial Neural Networks*, Encyclopedia of Physical Science and Technology (Third Edition), Academic Press, pp. 631-645, 2003. [CrossRef] [Google Scholar] [Publisher Link]

[68] Nikos D. Lagaros, "Artificial Neural Networks Applied in Civil Engineering," *Applied Sciences*, vol. 13, no. 2, pp. 1-8, 2023. [CrossRef] [Google Scholar] [Publisher Link]

[69] Fulin Li, Yuanbin Song, and Yongwei Shan, "Joint Extraction of Multiple Relations and Entities from Building Code Clauses," *Applied Sciences*, vol. 10, no. 20, pp. 1-18, 2020. [CrossRef] [Google Scholar] [Publisher Link]

[70] Nabil Mekaoui, and Taiki Saito, "A Deep Learning-Based Integration Method for Hybrid Seismic Analysis of Building Structures: Numerical Validation," *Applied Sciences*, vol. 12, no. 7, pp. 1-21, 2022. [CrossRef] [Google Scholar] [Publisher Link]

[71] Chen Xiong et al., "Multiple-Input Convolutional Neural Network Model for Large-Scale Seismic Damage Assessment of Reinforced Concrete Frame Buildings," *Applied Sciences*, vol. 11, no. 17, pp. 1-20, 2021. [CrossRef] [Google Scholar] [Publisher Link]

[72] Mohamed Ahzam Amanullah et al., "Deep Learning and Big Data Technologies for IoT Security," *Computer Communications*, vol. 151, pp. 495-517, 2020. [CrossRef] [Google Scholar] [Publisher Link]

[73] Nikos Ath. Kallioras, Alexandros N. Nordas, and Nikos D. Lagaros, "Deep Learning-Based Accuracy Upgrade of Reduced Order Models in Topology Optimization," *Applied Sciences*, vol. 11, no. 24, pp. 1-19, 2021. [CrossRef] [Google Scholar] [Publisher Link]

[74] Ronald Roberts, Laura Inzerillo, and Gaetano Di Mino, "Exploiting Data Analytics and Deep Learning Systems to Support Pavement Maintenance Decisions," *Applied Sciences*, vol. 11, no. 6, pp. 1-27, 2021. [CrossRef] [Google Scholar] [Publisher Link]

[75] Yu Ding et al., "Study on Two-Phase Fluid-Solid Coupling Characteristics in Saturated Zone of Subgrade Considering the Effects of Fine Particles Migration," *Applied Sciences*, vol. 10, no. 21, pp. 1-22, 2020. [CrossRef] [Google Scholar] [Publisher Link]

[76] Assia Aboubakar Mahamat et al., "Machine Learning Approaches for Prediction of the Compressive Strength of Alkali Activated Termite Mound Soil," *Applied Sciences*, vol. 11, no. 11, pp. 1-13, 2021. [CrossRef] [Google Scholar] [Publisher Link]

[77] Nan-Jing Wu, "Predicting the Compressive Strength of Concrete Using an RBF-ANN Model," *Applied Sciences*, vol. 11, no. 14, pp. 1-10, 2021. [CrossRef] [Google Scholar] [Publisher Link]

[78] Pratishtha Mishra, Pijush Samui, and Elham Mahmoudi, "Probabilistic Design of Retaining Wall Using Machine Learning Methods," *Applied Sciences*, vol. 11, no. 12, pp. 1-14, 2021. [CrossRef] [Google Scholar] [Publisher Link]

[79] Dong-Wook Oh et al., "Prediction of Change Rate of Settlement for Piled Raft Due to Adjacent Tunneling Using Machine Learning," *Applied Sciences*, vol. 11, no. 13, pp. 1-25, 2021. [CrossRef] [Google Scholar] [Publisher Link]

[80] Manuel Saldaña et al., "Applying Statistical Analysis and Machine Learning for Modeling the UCS from P-Wave Velocity, Density and Porosity on Dry Travertine," *Applied Sciences*, vol. 10, no. 13, pp. 1-14, 2020. [CrossRef] [Google Scholar] [Publisher Link]

[81] D. Cóstola, B. Blocken, and J.L.M. Hensen, "Overview of Pressure Coefficient Data in Building Energy Simulation and Airflow Network Programs," *Building and Environment*, vol. 44, no. 10, pp. 2027-2036, 2009. [CrossRef] [Google Scholar] [Publisher Link]

[82] Mohammad I. Al Biajawi et al., "Recycled Coal Bottom Ash as Sustainable Materials for Cement Replacement in Cementitious Composites: A Review," *Construction and Building Materials*, vol. 338, 2022. [CrossRef] [Google Scholar] [Publisher Link]

[83] Mehmet Serkan Kırgız, and Hasan Biricik, *1 - Wheat Straw Ash as Hydraulic Binder Substitution in Binder-Based Materials Made of an Admixture Superplasticizer*, Advance Upcycling of By-Products in Binder and Binder-Based Materials, Woodhead Publishing, pp. 1-23, 2024. [CrossRef] [Google Scholar] [Publisher Link]

[84] S. Stach, *11 - Modelling Fracture Processes in Orthopaedic Implants*, *Computational Modelling of Biomechanics and Biotribology in the Musculoskeletal System*, Woodhead Publishing, pp. 331-368, 2014. [CrossRef] [Google Scholar] [Publisher Link]

[85] S. Kenai, B. Benabed, and H. Soualhi, *9 - Marble Powder as Hydraulic Binder Substitution*, *Advance Upcycling of By-Products in Binder and Binder-Based Materials*, Woodhead Publishing, pp. 167-202, 2024. [CrossRef] [Google Scholar] [Publisher Link]

[86] "*NZS 4297:1998: Engineering Design of Earth Buildings*," Standards New Zealand, Wellington, pp. 1-62, 1998. [Google Scholar] [Publisher Link]

[87] "*Rammed Earth Structures - Code of Practice THC 03*," African Organisation for Standardisation, pp. 1-46, 2014. [Publisher Link]

[88] G.F. Middleton, and L.M. Schneider, *Earth-Wall Construction*, National Building Technology Centre, pp. 1-65, 1987. [Google Scholar] [Publisher Link]

[89] Peter Walker, *The Australian Earth Building Handbook*, Standards Australia International, pp. 1-152, 2002. [Google Scholar] [Publisher Link]

[90] *14-Housing and Construction Chapter 7 Building Codes General*, pp. 1-31, 2009. [Google Scholar] [Publisher Link]

[91] M.H. Faber, and J.D. Sørensen, "Reliability Based Code Calibration," *JCSS Workshop*, Zurich, Switzerland, pp. 1-19, 2002. [Google Scholar] [Publisher Link]

[92] Luis G.L. Costa, and André T. Beck, "A Critical Review of Probabilistic Live Load Models for Buildings: Models, Surveys, Eurocode Statistics and Reliability-Based Calibration," *Structural Safety*, vol. 106, pp. 2024. [CrossRef] [Google Scholar] [Publisher Link]

[93] H. Gulvanessian, "EN1990 Eurocode-Basis of Structural Design," *Proceedings of the Institution of Civil Engineers - Civil Engineering*, vol. 144, no. 6, pp. 8-13, 2001. [CrossRef] [Google Scholar] [Publisher Link]

[94] H. Nfaoui, J. Buret, and A.A.M. Sayigh, "Wind Characteristics and Wind Energy Potential in Morocco," *Solar Energy*, vol. 63, no. 1, pp. 51-60, 1998. [CrossRef] [Google Scholar] [Publisher Link]

[95] V.M. Khokhlov, and Y.E. Hadri, "Spatiotemporal Distribution of Wind Speed and Daily Maximum Wind Speed Indicators in Morocco in 2020-2050," *Bulletin of Taras Shevchenko National University of Kyiv*, *Geography*, pp. 68-71, 2018. [CrossRef] [Google Scholar] [Publisher Link]

[96] Youssef El Hadri, and Valeriy Khokhlov, "Wind Speed Regime in Tangier in 2021-2050," *Ukrainian Hydrometeorological Journal*, pp. 5-13, 2019. [CrossRef] [Google Scholar] [Publisher Link]

[97] E. Baglioni, L. Rovero, and U. Tonietti, *The Moroccan Drâa Valley Earthen Architecture: Pathology and Intervention Criteria*, 1st ed., Rammed Earth Conservation, CRC Press, pp. 1-6, 2012. [Google Scholar] [Publisher Link]

[98] Q.B. Bui et al., "First Exploratory Study on Dynamic Characteristics of Rammed Earth Buildings," *Engineering Structures*, vol. 33, no. 12, pp. 3690-3695, 2011. [CrossRef] [Google Scholar] [Publisher Link]

[99] "*Nepal National Building Code NBC 204:2015*, *Guidelines for Earthquake Resistant Building Construction: Earthen Building*," Department of Urban Development and Building Construction, Babar Mahal, Kathmandu, Nepal, pp. 1-80, 2015. [Publisher Link]

[100] Ranime El-Nabouch et al., "Assessing the In-plane Seismic Performance of Rammed Earth Walls by Using Horizontal Loading Tests," *Engineering Structures*, vol. 145, pp. 153-161, 2017. [CrossRef] [Google Scholar] [Publisher Link]

[101] Q.B. Bui et al., "Vertical Rods as a Seismic Reinforcement Technique for Rammed Earth Walls: An Assessment," *Advances in Civil Engineering*, vol. 2019, pp. 1-12, 2019. [CrossRef] [Google Scholar] [Publisher Link]

[102] Anand S. Arya, "*Guidelines for Earthquake Resistant Design, Construction and Retrofitting of Buildings in Afghanistan*," Nations Centre for Regional Development, pp. 1-162, 2003. [Google Scholar] [Publisher Link]

[103] "*IS 13827 (1993): Indian Standard, Improving Earthquake Resistance of Earthen Buildings – Guidelines*," Bureau of Indian Standards, pp. 1-23, 1993. [Google Scholar] [Publisher Link]

[104] "*Federal Republic of Nigeria: National Building Code*," LexisNexis Butterworths, Minister of Housing and Urban Development Abuja, pp. 1-476, 2006. [Google Scholar] [Publisher Link]

[105] M. Ramezanpour, A. Eslami, and H. Ronagh, "Seismic Performance of Stabilised/unstabilised Rammed Earth Walls," *Engineering Structures*, vol. 245, pp. 1-32, 2021. [CrossRef] [Google Scholar] [Publisher Link]

[106] Alric Lucas, Guy Pluvinage, and Capelle Julien, "Reliability Index of a Pipe Transporting Hydrogen Submitted to Seismic Displacement," *International Journal of Pressure Vessels and Piping*, vol. 208, 2024. [CrossRef] [Google Scholar] [Publisher Link]

[107] Mark G. Stewart, and Stephen James Lawrence, "Structural Reliability of Masonry Walls in Flexure," *International Masonry Society*, vol. 15, 2002. [Google Scholar] [Publisher Link]

[108] Marco Liu, "*Optimal Number of Trials for Monte Carlo Simulation*," Valuation Research Report 1065, pp. 1-3, 2017. [Google Scholar] [Publisher Link]

[109] Ana-Maria Simundic, "Confidence Interval," *Biochemica Medica*, vol. 18, no. 2, pp. 154-161, 2008. [CrossRef] [Google Scholar] [Publisher Link]

[110] Luke Akong'o Orawo, "Confidence Intervals for the Binomial Proportion: A Comparison of Four Methods," *Open Journal of Statistics*, vol. 11, no. 5, pp. 806-816, 2021. [CrossRef] [Google Scholar] [Publisher Link]

[111] Weiwei Jiang, "Applications of Deep Learning in Stock Market Prediction: Recent Progress," *Expert Systems with Applications*, vol. 184, pp. 1-97, 2021. [CrossRef] [Google Scholar] [Publisher Link]

[112] Roman Kern et al., *Chapter 14 - Astro- and Geoinformatics – Visually Guided Classification of Time Series Data*, Knowledge Discovery in Big Data from Astronomy and Earth Observation, Astrogeoinformatics, pp. 267-282, 2020. [CrossRef] [Google Scholar] [Publisher Link]

[113] Aurelien Teguede Keleko et al., "Health Condition Monitoring of a Complex Hydraulic System Using Deep Neural Network and DeepSHAP Explainable XAI," *Advances in Engineering Software*, vol. 175, pp. 1-24, 2023. [CrossRef] [Google Scholar] [Publisher Link]

[114] Y.S. Park, and S. Lek, *Chapter 7 - Artificial Neural Networks: Multilayer Perceptron for Ecological Modeling*, Developments in Environmental Modelling, vol. 28, pp. 123-140, 2016. [CrossRef] [Google Scholar] [Publisher Link]

[115] S.J. ELLIOTT, *8 - Active Control of Nonlinear Systems*, Signal Processing for Active Control, Academic Press, pp. 367-409, 2001. [CrossRef] [Google Scholar] [Publisher Link]

[116] Henri P. Gavin, "*The Levenberg-Marquardt Algorithm for Nonlinear Least Squares Curve-Fitting Problems*," Department of Civil and Environmental Engineering Duke University, pp. 1-23, 2024. [Google Scholar] [Publisher Link]

[117] Ananth Ranganathan, "*The Levenberg-Marquardt Algorithm*," Tutoral on LM Algorithm, pp. 1-5, 2004. [Google Scholar] [Publisher Link]

[118] Fareed Jumah et al., "Uncharted Waters of Machine and Deep Learning for Surgical Phase Recognition in Neurosurgery," *World Neurosurgery*, vol. 160, pp. 4-12, 2022. [CrossRef] [Google Scholar] [Publisher Link]

[119] Farhad Maleki et al., "Machine Learning Algorithm Validation: From Essentials to Advanced Applications and Implications for Regulatory Certification and Deployment," *Neuroimaging Clinics of North America*, vol. 30, no. 4, pp. 433-445, 2020. [CrossRef] [Google Scholar] [Publisher Link]

[120] Daniel Berrar, *Cross-Validation*, Encyclopedia of Bioinformatics and Computational Biology, Elsevier, vol. 1, pp. 542-545, 2019. [CrossRef] [Google Scholar] [Publisher Link]